Understanding the Magnetic Polarizability Tensor

Paul D. Ledger[1] and W. R. Bill Lionheart[2]

[1]College of Engineering, Swansea University Bay Campus, Swansea SA1 8EN, U.K.
[2]School of Mathematics, The University of Manchester, Manchester M13 9PL, U.K.

The aim of this paper is to provide new insights into the properties of the rank 2 polarizability tensor $\overset{\approx}{\mathcal{M}}$ proposed by Ledger and Lionheart for describing the perturbation in the magnetic field caused by the presence of a conducting object in the eddy-current regime. In particular, we explore its connection with the magnetic polarizability tensor and the Pólya–Szegö tensor and how, by introducing new splittings of $\overset{\approx}{\mathcal{M}}$, they form a family of rank 2 tensors for describing the response from different categories of conducting (permeable) objects. We include new bounds on the invariants of the Pólya–Szegö tensor and expressions for the low-frequency and high-conductivity limiting coefficients of $\overset{\approx}{\mathcal{M}}$. We show, for the high-conductivity case (and for frequencies at the limit of the quasi-static approximation), that it is important to consider whether the object is simply or multiply connected but, for the low-frequency case, the coefficients are independent of the connectedness of the object. Furthermore, we explore the frequency response of the coefficients of $\overset{\approx}{\mathcal{M}}$ for a range of simply and multiply connected objects.

Index Terms—**Eddy currents, land mine detection, magnetic induction, metal detectors, polarizability tensors.**

I. Introduction

THE NEED to detect and characterize the conducting targets from magnetic induction measurements arises in a wide range of applications, most notably in metal detection. Here, one wishes to be able to locate and identify a highly conducting object in a low-conducting background. Applications include ensuring safety at airports and at public events, maintaining quality in the mechanized production of food as well as in the detection of unexploded ordnance and land mines and in archeological surveys. Furthermore, there is interest in producing conductivity images from multiple magnetic induction measurements, most notably in magnetic induction tomography for medical applications [18], [46] and industrial applications [16], [42]. Eddy currents also have important applications in non-destructive testing, such as investigating the integrity of reinforced concrete structures and bridges [41].

In the engineering literature [14], [31], [35], [37], the signal induced by an alternating low-frequency magnetic field, due to the presence of a conducting (permeable) object, located at position z, is often postulated as

$$V^{\text{ind}} \approx \boldsymbol{H}_0^m \cdot \left(\mathcal{A}\boldsymbol{H}_0^e\right) \tag{1}$$

where only $\boldsymbol{H}_0^m$ and $\boldsymbol{H}_0^e$ depend on position, $\boldsymbol{H}_0^e := \boldsymbol{H}_0(z)$ is the background magnetic field generated by passing a current though an excitor coil placed away from the object, evaluated at the position of the center of the object, and $\boldsymbol{H}_0^m$ is the corresponding field that would be evaluated by passing a unit current through the measurement coil, evaluated at the same location. The object

$$\mathcal{A} = \sum_{i=1}^{3}\sum_{j=1}^{3} \mathcal{A}_{ij}\hat{\boldsymbol{e}}_i \otimes \hat{\boldsymbol{e}}_j \tag{2}$$

has been proposed to be a (complex) symmetric rank 2 magnetic polarizability tensor described by six independent empirically fitted complex coefficients $\mathcal{A}_{ij}$ containing information about the shape, material properties, and frequency response of an object. The coefficients are independent of its position, and $\hat{\boldsymbol{e}}_i$, $i = 1, 2, 3$ are the unit basis vectors for the chosen coordinate system.

In the applied mathematics literature [2], [4]–[6], [24], [25], [28], asymptotic formulas are available that describe the perturbation in the magnetic field due to the presence of a magnetic (conducting) object B_α using Einstein's summation convention in the form

$$((\boldsymbol{H}_\alpha - \boldsymbol{H}_0)(\boldsymbol{x}))_i = \left(\boldsymbol{D}_{\boldsymbol{x}}^2 G(\boldsymbol{x}, z)\right)_{ij}\mathcal{A}_{jk}(\boldsymbol{H}_0(z))_k + (\boldsymbol{R}(\boldsymbol{x}))_i \tag{3}$$

as some suitable limit is taken. In the above, $B_\alpha = \alpha B + z$, which means that the physical object can be expressed in terms of a unit object B placed at the origin, scaled by the object size α and translated by the vector z, $\boldsymbol{R}(\boldsymbol{x})$ is a residual vector, and $G(\boldsymbol{x}, z) := 1/(4\pi|\boldsymbol{x} - z|)$ is the free space Laplace Green's function and

$$\begin{aligned}\left(\boldsymbol{D}_{\boldsymbol{x}}^2 G(\boldsymbol{x}, z)\right)_{ij} &= \left(\boldsymbol{D}_{\boldsymbol{x}}^2 G(z, \boldsymbol{x})\right)_{ij} \\ &= \frac{1}{4\pi r^3}(3\hat{\boldsymbol{r}}_i\hat{\boldsymbol{r}}_j - \delta_{ij})\end{aligned} \tag{4}$$

with $\boldsymbol{r} := \boldsymbol{x} - z$, $r = |\boldsymbol{r}|$, $\hat{\boldsymbol{r}} = \boldsymbol{r}/r$ and δ_{ij} are the coefficients of the unit tensor. For these asymptotic formulas, the form of $\mathcal{A}_{jk}$ is explicitly known and is computable by solving a transmission problem. It is easily established that this is exactly of the form $\boldsymbol{H}_0^m \cdot (\mathcal{A}\boldsymbol{H}_0^e)$ given in (1). This is done by idealizing the background magnetic field as that produced by a magnetic dipole and then taking the component

Manuscript received October 16, 2015; revised November 27, 2015; accepted December 4, 2015. Corresponding author: P. D. Ledger (e-mail: p.d.ledger@swansea.ac.uk).

Color versions of one or more of the figures in this paper are available online at http://ieeexplore.ieee.org.

Digital Object Identifier 10.1109/TMAG.2015.2507169

of (3) in the direction of the magnetic moment associated with the background magnetic field that would result from the measurement coil being treated as an excitor.

In this paper, we will explore the connection between the empirically fitted engineering polarizability tensor and the asymptotic expansions combined with the different expressions for polarization tensor that appear in the applied mathematics literature. In particular, we advocate that an asymptotic formula for the perturbed magnetic field provides greater insight than (1) for the following reasons. If the empirical approach is followed, the coefficients of the polarizability tensor are obtained by taking measurements (or performing simulated measurements using a computational techniques, such as finite elements) in order to determine the voltage at different positions for different excitor combinations and then use a least squares approach to approximately determine the coefficients $\mathcal{A}_{ij}$ [14], [31], [35], [37]. It is important to ensure that the measurements are taken in different planes and at distances from the object in order to capture the correct asymptotic behavior; however, the presence of measurement noise can make this challenging to achieve in practice. Furthermore, the number of measurements should greatly exceed the number of coefficients to be determined in order to minimize any measurement errors. For each new object, i.e., a different shape, frequency, or material property, this measurement procedure must be repeated in order to determine the polarizability tensor. An asymptotic formula, on the other hand, provides an explicit expression that allows the tensor to be computed without the need for performing (or simulating) measurements. Indeed, perhaps a contributing factor as to why this approach has not been persued among engineers so far is that the term polarization tensor is preferred in the applied mathematics literature for $\mathcal{A}$, while, in the engineering community, the term polarizability tensor is more commonly adopted. Another benefit is that rather than knowing that the voltage is only approximately given (1), without knowing its accuracy, we have, through (3), not only the leading term but also a way of rigorously describing the remainder.

The availability of explicit expressions for different classes of polarization/polarizability tensors makes it possible to investigate their properties, such as the reduction in the number of independent coefficients for rotational and reflectional symmetries of the object, which we considered in [28]. In this paper, we provide the following novel contributions, which further enhance the understanding of their properties. First, we review the different forms that the tensors can take for magnetic and conducting (permeable) objects as part of asymptotic expansions of the perturbed magnetic field when either the object size or the frequency tends to zero. Second, we present new bounds on the invariants of some classes of the tensors and provide bounds on the spherical and deviatoric parts of the tensor for a magnetic object. Third, we present new results that describe the low-frequency and high-conductivity limits of the coefficients of the tensor for a conducting (permeable) object in an alternating background magnetic field. We consider the response from magnetic and conducting ellipsoids and, finally, the response from a conducting Remington rifle cartridge as a practical application of the aforementioned theory.

The presentation of the material is organized as follows. In Section II, we summarize the low-frequency and eddy-current models and then, in Section III, we consider explicit expressions for the polarization/polarizability tensors for magnetic and conducting (permeable) objects and, in the latter case, present a new splitting of the tensor. In Section IV, we present bounds on the properties of the tensors and then, in Section V, we consider the limiting case of low frequency and high conductivity for the coefficients of the tensor. Section VI describes the response from magnetic and conducting ellipsoids, and in Section VIII, the response from a conducting Remington rifle cartridge is described as a practical application of the aforementioned theory. We conclude the presentation with some concluding remarks in Section IX.

II. Mathematical Models

Following [2], we let $\mathbb{R}^3$ denote the Euclidean space and introduce the position-dependent material parameters as:

$$\epsilon_\alpha = \begin{cases} \epsilon_* \\ \epsilon_0, \end{cases} \qquad \mu_\alpha = \begin{cases} \mu_* \\ \mu_0, \end{cases} \qquad \sigma_\alpha = \begin{cases} \sigma_* & \text{in } B_\alpha \\ 0 & \text{in } \mathbb{R}^3 \backslash B_\alpha \end{cases} \tag{5}$$

where ϵ, μ, and σ are the permittivity, permeability and conductivity, respectively, and the subscript 0 refers in the former cases to the free space values. We remark that the background medium is assumed to be non-conducting free space, which is a reasonable approximation to make for buried objects in dry ground provided that the contrast between the object and the surrounding material is sufficiently high.

Low-frequency electromagnetic scattering problems are described in terms of the (total) time harmonic $\boldsymbol{E}_\alpha$ and $\boldsymbol{H}_\alpha$ for angular frequency ω, which result from the interaction between the background (incident) fields $\boldsymbol{E}_0$ and $\boldsymbol{H}_0$ and the object B_α. These fields satisfy the equations

$$\nabla \times \boldsymbol{E}_\alpha = \mathrm{i}\omega\mu_\alpha \boldsymbol{H}_\alpha \quad \text{in } \mathbb{R}^3 \tag{6a}$$

$$\nabla \times \boldsymbol{H}_\alpha = \sigma_\alpha \boldsymbol{E}_\alpha - \mathrm{i}\omega\epsilon_\alpha \boldsymbol{E}_\alpha \quad \text{in } \mathbb{R}^3 \tag{6b}$$

and suitable radiation conditions as $|\boldsymbol{x}| \to \infty$ where $\mathrm{i} := \sqrt{-1}$. The background fields $\boldsymbol{E}_0$ and $\boldsymbol{H}_0$ satisfy the free space version of the above equations (i.e., replacing the subscript α with 0).

In the eddy-current model, the geometry, frequency, and material parameters are such that the displacement currents in the Maxwell system can be neglected. This is often justified on the basis that $(\epsilon_*\mu_*)^{1/2}\alpha\omega \ll 1$ or $\epsilon_*\omega/\sigma_* \ll 1$. A more rigorous justification of the eddy-current model appears in [1]. In [39], the effect of the shape of the conductor on the validity of the eddy-current model is discussed. The depth of penetration of the magnetic field in a conducting object is described by its skin depth, $s := (2/(\omega\mu_0\sigma_*))^{1/2}$, and by introducing a parameter $\nu := 2\alpha^2/s^2$, the mathematical model of interest in this case refers to when $\nu = O(1)$[1] and $\mu_*/\mu_0 = O(1)$ as $\alpha \to 0$ [2]. When considering the eddy-current model, the time-harmonic fields $\boldsymbol{E}_\alpha$ and $\boldsymbol{H}_\alpha$ are

[1]Where $f(x) = O(g(x))$ if and only if there is a positive constant M, such that $|f(x)| < M|g(x)|$ for all sufficiently large x, i.e., $x \geqslant x_0$. This is known as Landau big O notation.

those that result from a time varying current source located away from B_α, with volume current density $\boldsymbol{J}_0$ and $\nabla \cdot \boldsymbol{J}_0 = 0$ in $\mathbb{R}^3$, and their interaction with the object B_α, and satisfy the equations

$$\nabla \times \boldsymbol{E}_\alpha = \mathrm{i}\omega\mu_\alpha \boldsymbol{H}_\alpha \quad \text{in } \mathbb{R}^3 \tag{7a}$$

$$\nabla \times \boldsymbol{H}_\alpha = \sigma_\alpha \boldsymbol{E}_\alpha + \boldsymbol{J}_0 \quad \text{in } \mathbb{R}^3 \tag{7b}$$

together with a suitable static decay rate of the fields as $|\boldsymbol{x}| \to \infty$ [1]. In this case, in the absence of an object, the background magnetic field, $\boldsymbol{H}_0$, is that generated by the current source.

III. Asymptotic Formulas and Explicit Expressions for Polarization Tensors

In Section III-A, we discuss as asymptotic expressions for the perturbed magnetic field $(\boldsymbol{H}_\alpha - \boldsymbol{H}_0)(\boldsymbol{x})$ for the mathematical model described by (6). Then, in Section III-B, we present the expansions for the mathematical model described by (7). In Section III-C, we consider the connection between these results.

A. Asymptotic Expansions for Equation System (6)

For dielectric, magnetic and perfectly conducting objects whose dimensions are small compared with the wavelength, i.e., $\kappa\alpha$ small, where $\kappa := \omega\sqrt{\epsilon_0\mu_0}$ is the free space wave number and α is the object size, it is well known that the scattering caused by the presence of the inclusion in a background field can be approximated by a dipole expansion, and in the case of a sphere, explicit expressions for the induced dipole moments are available [20, pp. 413–415]. These induced dipole moments can be expressed as the product of a diagonal rank 2 tensor and the background field, evaluated at the position of the object. Similar results are also available for dielectric and magnetic spheres in uniform static fields [20, p. 151]. The ability to describe the induced dipole moments in terms of rank 2 (polarization/polarizability) tensors for other shapes has also been reported [27, p. 54], [34, p. 1886],[2] where it is proposed that the tensors are symmetric and a function of both the object's shape and its material properties, but without an explicit expression for the general case. A further difficulty, with describing the scattered fields by dipole expansions, is how small $\kappa\alpha$ needs to be for a good approximation, and an asymptotic expansion, on the other hand, quantifies the remainder term.

For fixed α, the asymptotic expansions of Kleinman [24], [25] present the leading-order terms for the perturbed in terms of the dipole moments for the case when $\kappa \to 0$ and $r \to \infty$, where r is the distance from the object to the point of observation. By considering the leading-order terms, he is able to express the electric and magnetic dipole moments as linear combinations of the background field through dielectric and magnetic polarization/polarizability tensors, with explicit expressions for the tensor coefficients [15], [22], [26]. Our recent work [29] includes not only the terms as $r \to \infty$, but also includes those at distances that are large compared with the size of the object. In particular, by considering the case of fixed r and α, this reduces to

$$((\boldsymbol{H}_\alpha - \boldsymbol{H}_0)(\boldsymbol{x}))_i = \left(\boldsymbol{D}^2_{\boldsymbol{x}} G(\boldsymbol{x}, \boldsymbol{z})\right)_{ij} \mathcal{T}(\mu_r)_{jk} (\boldsymbol{H}_0(\boldsymbol{z}))_k + (\mathbf{R}(\mathbf{x}))_i \tag{8}$$

where $\boldsymbol{R}(\boldsymbol{x}) = O(\kappa)$ as $\kappa \to 0$ for a simply connected smooth inclusion with permeability contrast $\mu_r := \mu_*/\mu_0$ at points away from the object, which describes the magnetostatic response as the limiting case of a low-frequency scattering problem. If we do not fix r and α, [29, Th. 4.2] can also describe the scattering from dielectric objects at distances that are large compared with the object size, but not the response from conducting objects. The real symmetric rank 2 tensor $\mathcal{T}(\mu_r)$ can be expressed in range of different forms [15], [22], [26] and can, in fact, be identified with the Pólya–Szegö tensor [4], whose coefficients are explicitly given by

$$\mathcal{T}(\mu_r)_{ij} = \alpha^3 \left((\mu_r - 1)|B|\delta_{ij} + (\mu_r - 1)^2 \int_\Gamma \hat{\boldsymbol{n}}^- \cdot (\nabla_{\boldsymbol{\xi}} \phi_i) \xi_j d\boldsymbol{\xi} \right) \tag{9}$$

where $\xi_j = (\boldsymbol{\xi})_j$ with $\boldsymbol{\xi}$ measured from the center of B. In the above, ϕ_i, $i = 1, 2, 3$, satisfies the transmission problem

$$\nabla^2 \phi_i = 0 \quad \text{in } B \cup B^c \tag{10a}$$

$$[\phi_i]_\Gamma = 0 \quad \text{on } \Gamma \tag{10b}$$

$$\hat{\boldsymbol{n}} \cdot \nabla \phi_i|_+ - \hat{\boldsymbol{n}} \cdot \nabla \mu_r \phi_i|_- = \hat{\boldsymbol{n}} \cdot \nabla \xi_i \quad \text{on } \Gamma \tag{10c}$$

$$\phi_i \to 0 \quad \text{as } |\boldsymbol{\xi}| \to \infty \tag{10d}$$

where Γ is the interface between B and B^c and $[\cdot]_\Gamma$ denotes the jump across Γ. Here, and in the sequel, we have dropped the subscript $\boldsymbol{\xi}$ on ∇ and $\boldsymbol{x}$ on $\boldsymbol{D}$ unless confusion may arise. Note that other forms of $\mathcal{T}(\mu_r)_{ij}$ are possible, and in [29], we show the equivalence of some common arrangements. By taking appropriate limiting values of μ_r, the far field perturbation caused by the presence of a perfectly conducting object can also be described [15], [26].

By contrast, the asymptotic behavior of scattering by a small smooth simply connected object has been obtained on bounded [5], [45] and unbounded domains [6], [29] and, for the limiting magnetostatic response given by $\kappa = 0$, has a similar form to (8) with $\boldsymbol{R}(\boldsymbol{x}) = O(\alpha^3)$ as $\alpha \to 0$. When $\kappa \neq 0$, these results also include additional terms, which also describe the scattering from a conducting dielectric object in terms of $\mathcal{T}(\epsilon_r^c)$, where $\epsilon_r^c := (\epsilon_* - \mathrm{i}\sigma_*/\omega)/\epsilon_0$.

B. Asymptotic Expansions for Equation System (7)

In the above, we have described a series of different asymptotic expansions, which although having a similar form to (3), and describing the perturbed fields for smooth simply connected magnetic objects in the magnetostatic regime (as the limiting cases of electromagnetic scattering problems), do not describe the response from conducting objects in the quasi-static regime, i.e., the eddy-current problem. The existence of a relationship of the form (1) for the case

[2]For a discussion on the polarizability of molecules [27], however, this outside the scope of this paper.

of a conducting sphere in the eddy-current regime was first shown by Wait [44]. For this case, $\mathcal{A}$ is diagonal, and he claimed that such a relationship could potentially be used for identifying the conductivity and the radius of a sphere. Landau and Lifshitz [27, p. 192] proposed that the magnetic moment acquired by the conductor in a magnetic field can be expressed in terms of the product of a symmetric magnetic polarizability tensor and the background field.[3] Subsequently, Järvi [21] and, independently, Baum [9], [10] have proposed that (1) holds for general-shaped conducting objects.[4] Moreover, to the best of our knowledge, with the exception of the sphere, an explicit expression for computing the coefficients of the magnetic polarizability for a conducting object is not available and this has led to the common engineering approach of empirically fitting their coefficients [14], [31], [35], [37].

Ammari *et al.* [2] have recently obtained an asymptotic expansion, which, for the first time, correctly describes the perturbed magnetic field as $\alpha \to 0$ for a conducting (possibly also permeable and multiply connected) object in the presence of a low-frequency background magnetic field, generated by a coil with an alternating current. In [3], further useful calculations and a dictionary-based classification algorithm for identifying conducting objects are presented. We quote the result of [2, Th. 3.2] in the alternative manner, as first stated in [28]

$$(\boldsymbol{H}_\alpha - \boldsymbol{H}_0)(\boldsymbol{x})_i = (\boldsymbol{D}^2 G(\boldsymbol{x}, z))_{\ell m} \mathcal{M}_{\ell m i j} (\boldsymbol{H}_0(z))_j + O(\alpha^4) \tag{11}$$

as $\alpha \to 0$. At first glance, this appears similar to the result stated in (3); however, note that the result is expressed in terms of a rank 4 tensor, which appears as an inner product with $\boldsymbol{D}^2 G(\boldsymbol{x}, z)$ over the first two indices. Moreover, a rank 4 tensor can have as many as 64 independent complex coefficients $\mathcal{M}_{\ell m j i}$, whereas for a symmetric rank 2 tensor, this can have at most six independent complex coefficients. In [28], we show that for a right-handed orthonormal coordinate system, described by the unit vectors $\hat{\boldsymbol{e}}_j$, $j = 1, 2, 3$, which are chosen as the Cartesian coordinate directions, then it is possible to reduce this result to

$$(\boldsymbol{H}_\alpha - \boldsymbol{H}_0)(\boldsymbol{x})_i = (\boldsymbol{D}^2 G(\boldsymbol{x}, z))_{ij} \overset{\approx}{\mathcal{M}}_{jk} (\boldsymbol{H}_0(z))_k + O(\alpha^4) \tag{12}$$

as $\alpha \to 0$, where $\overset{\approx}{\mathcal{M}}$ is a complex symmetric rank 2 tensor, which we, henceforth, denote as the magnetic polarizability tensor.[5] For consistency with [28], we use a single check to denote the reduction in a tensor's rank by 1 and a single hat to denote its extension in rank by 1. The coefficients of $\overset{\approx}{\mathcal{M}}$ are defined as $\overset{\approx}{\mathcal{M}}_{ij} := \mathcal{N}_{ij} - \check{\mathcal{C}}_{ij}$, where

$$\check{\mathcal{C}}_{ij} := -\frac{\mathrm{i}\nu\alpha^3}{4} \hat{\boldsymbol{e}}_i \cdot \int_B \boldsymbol{\xi} \times (\boldsymbol{\theta}_j + \hat{\boldsymbol{e}}_j \times \boldsymbol{\xi}) d\boldsymbol{\xi} \tag{13a}$$

$$\mathcal{N}_{ij} := \alpha^3 \left(1 - \frac{\mu_0}{\mu_*}\right) \int_B \left(\hat{\boldsymbol{e}}_i \cdot \hat{\boldsymbol{e}}_j + \frac{1}{2} \hat{\boldsymbol{e}}_i \cdot \nabla \times \boldsymbol{\theta}_j\right) d\boldsymbol{\xi} \tag{13b}$$

and $\boldsymbol{\theta}_i$ solves the vector valued transmission problem

$$\begin{aligned}
\nabla \times \mu^{-1} \nabla \times \boldsymbol{\theta}_i - \mathrm{i}\omega\sigma\alpha^2 \boldsymbol{\theta}_i &= \mathrm{i}\omega\sigma\alpha^2 \hat{\boldsymbol{e}}_i \times \boldsymbol{\xi} \quad \text{in } B \cup B^c && \text{(14a)}\\
\nabla \cdot \boldsymbol{\theta}_i &= 0 \quad \text{in } B^c && \text{(14b)}\\
[\boldsymbol{\theta}_i \times \hat{\boldsymbol{n}}]_\Gamma &= \boldsymbol{0}, \quad \text{on } \Gamma && \text{(14c)}\\
[\mu^{-1} \nabla \times \boldsymbol{\theta}_i \times \hat{\boldsymbol{n}}]_\Gamma &= -2[\mu^{-1}]_\Gamma \hat{\boldsymbol{e}}_i \times \hat{\boldsymbol{n}} \quad \text{on } \Gamma && \text{(14d)}\\
\boldsymbol{\theta}_i(\boldsymbol{\xi}) &= O(|\boldsymbol{\xi}|^{-1}) \quad \text{as } |\boldsymbol{\xi}| \to \infty. && \text{(14e)}
\end{aligned}$$

We emphasize that (11) and (12) provide a rigorous mathematical framework for the perturbed magnetic field for the eddy-current case, and (13) together with the solution of the transmission problem (14) now provides explicit expressions for the computation of the coefficients of the tensor $\overset{\approx}{\mathcal{M}}$. In [28], we present the numerical results for the computation of the tensor coefficients of different objects and describe how mirror and rotational symmetries of an object can be applied to reduce the number of independent coefficients of $\overset{\approx}{\mathcal{M}}$.

C. Unified Description for Small Objects

From Sections III-A and III-B, we observe that for small objects, $(\boldsymbol{H}_\alpha - \boldsymbol{H}_0)(\boldsymbol{x})$ has the form of (3) with $\boldsymbol{R}(\boldsymbol{x}) = O(\alpha^4)$ and $\mathcal{A} = \mathcal{T}(\mu_r)$ for the magnetostatic response and $\mathcal{A} = \overset{\approx}{\mathcal{M}}$ for the eddy-current case as $\alpha \to 0$. We now state a series of lemmas, which unifies their treatment and shows that the former is, in fact, a simplification of the latter. We start with an alternative form of $\overset{\approx}{\mathcal{M}}$.

Lemma 1: The coefficents of $\overset{\approx}{\mathcal{M}}$ can be expressed as $\overset{\approx}{\mathcal{M}}_{ij} = \mathcal{N}^{\sigma *}_{ij} + \mathcal{N}^0_{ij} - \check{\mathcal{C}}^{\sigma *}_{ij}$, where

$$\check{\mathcal{C}}^{\sigma *}_{ij} := -\frac{\mathrm{i}\nu\alpha^3}{4} \hat{\boldsymbol{e}}_i \cdot \int_B \boldsymbol{\xi} \times \left(\boldsymbol{\theta}^{(0)}_j + \boldsymbol{\theta}^{(1)}_j\right) d\boldsymbol{\xi} \tag{15a}$$

$$\mathcal{N}^{\sigma *}_{ij} := \frac{\alpha^3}{2} \left(1 - \frac{\mu_0}{\mu_*}\right) \int_B \left(\hat{\boldsymbol{e}}_i \cdot \nabla \times \boldsymbol{\theta}^{(1)}_j\right) d\boldsymbol{\xi} \tag{15b}$$

$$\mathcal{N}^0_{ij} := \frac{\alpha^3}{2} \left(1 - \frac{\mu_0}{\mu_*}\right) \int_B \left(\hat{\boldsymbol{e}}_i \cdot \nabla \times \boldsymbol{\theta}^{(0)}_j\right) d\boldsymbol{\xi} \tag{15c}$$

and $\mathcal{N}^{\sigma *} - \check{\mathcal{C}}^{\sigma *}$ is a complex symmetric rank 2 tensor and $\mathcal{N}^0$ is a real symmetric rank 2 tensor. The coefficients of these tensors depend on the solutions $\boldsymbol{\theta}^{(0)}_i$ and $\boldsymbol{\theta}^{(1)}_i$, $i = 1, 2, 3$, to the transmission problems

$$\begin{aligned}
\nabla \times \mu^{-1} \nabla \times \boldsymbol{\theta}^{(0)}_i &= \boldsymbol{0} \quad \text{in } B \cup B^c && \text{(16a)}\\
\nabla \cdot \boldsymbol{\theta}^{(0)}_i &= 0 \quad \text{in } B \cup B^c && \text{(16b)}\\
\left[\boldsymbol{\theta}^{(0)}_i \times \hat{\boldsymbol{n}}\right]_\Gamma &= \boldsymbol{0} \quad \text{on } \Gamma && \text{(16c)}\\
\left[\mu^{-1} \nabla \times \boldsymbol{\theta}^{(0)}_i \times \hat{\boldsymbol{n}}\right]_\Gamma &= \boldsymbol{0} \quad \text{on } \Gamma && \text{(16d)}\\
\boldsymbol{\theta}^{(0)}_i(\boldsymbol{\xi}) - \hat{\boldsymbol{e}}_i \times \boldsymbol{\xi} &= O(|\boldsymbol{\xi}|^{-1}) \quad \text{as } |\boldsymbol{\xi}| \to \infty && \text{(16e)}
\end{aligned}$$

[3] They justify that the term magnetic polarizability tensor being applicable to this case as it is associated with a magnetic dipole and is a generalized susceptibility.

[4] Although the connection is not explicit, these authors appear to combine the proposition of [27] and a dipole expansion of the field to recover this result.

[5] A more precise definition would be to say that $\overset{\approx}{\mathcal{M}}$ is the leading-order approximation to the magnetic polarizability tensor for small objects. In [28], we include examples to demonstrate numerically that the prerturbed field and, hence, the coefficients of $\overset{\approx}{\mathcal{M}}$ behave asymptotically as predicated by (12).

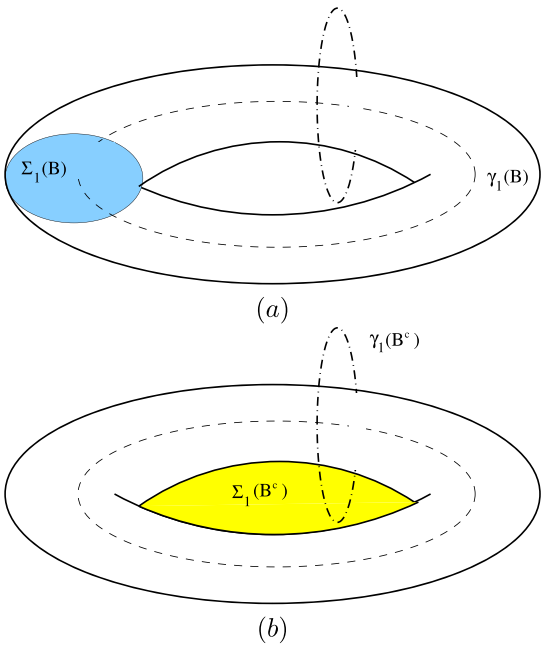

Fig. 1. Torus-shaped object B showing (a) typical non-bounding cycle $\gamma_1(B)$ and associated cutting surface $\Sigma_1(B)$ for B and (b) similar for B^c.

and

$$\begin{aligned}\nabla\times\mu^{-1}\nabla\times\boldsymbol{\theta}_i^{(1)}-\mathrm{i}\omega\sigma\alpha^2\big(\boldsymbol{\theta}_i^{(1)}+\boldsymbol{\theta}_i^{(0)}\big)&=\mathbf{0}\quad\text{in } B\cup B^c &(17a)\\ \nabla\cdot\boldsymbol{\theta}_i^{(1)}&=0\quad\text{in } B^c &(17b)\\ \big[\boldsymbol{\theta}_i^{(1)}\times\hat{\boldsymbol{n}}\big]_\Gamma&=\mathbf{0}\quad\text{on }\Gamma &(17c)\\ \big[\mu^{-1}\nabla\times\boldsymbol{\theta}_i^{(1)}\times\hat{\boldsymbol{n}}\big]_\Gamma&=\mathbf{0}\quad\text{on }\Gamma &(17d)\\ \boldsymbol{\theta}_i^{(1)}(\boldsymbol{\xi})&=O(|\boldsymbol{\xi}|^{-1})\quad\text{as } |\boldsymbol{\xi}|\to\infty. &(17e)\end{aligned}$$

Proof: The result immediately follows from the ansatz $\boldsymbol{\theta}_i=\boldsymbol{\theta}_i^{(0)}+\boldsymbol{\theta}_i^{(1)}-\hat{\boldsymbol{e}}_i\times\boldsymbol{\xi}$. The symmetries of $\mathcal{N}^{\sigma*}-\check{\mathcal{C}}^{\sigma*}$ and $\mathcal{N}^0$ follow similar arguments to [28, Proof of Lemma 4.4]. ■

To understand the role played by the topology of an object and its complement, we recall the definition of Betti numbers (see [11], [30], and references therein). The zeroth Betti number, $\beta_0(\Omega)$, is the number of connected parts of Ω, which for a bounded connected region in $\mathbb{R}^3$ is always 1. The first Betti number, $\beta_1(\Omega)$, is the genus, i.e., the number of handles, and the second Betti number $\beta_2(\Omega)$ is one less than the connected parts of the boundary $\partial\Omega$, i.e., the number of cavities. If we consider a situation where Ω has $\beta_1(\Omega)$ handles, then a non-bounding orientated path, $\gamma_i(\Omega)$, known as a loop, can be associated with each handle i. For $\beta_1(\Omega)$ loops, one can associate $\beta_1(\Omega)$ cuts of Ω that can be represented by Seifert surfaces as shown for the situation, where B is a solid torus in Fig. 1. If $(\Sigma_1\cup\cdots\cup\Sigma_N)$ where $N:=\beta_1(\Omega)$ stands for the complete set of cuts, we recall that a curl free field can only be represented by the gradient of a scalar field in $\Omega\backslash(\Sigma_1\cup\cdots\Sigma_N)$. Furthermore, we recall that a simply connected region has $\beta_0(\Omega)=1$ and $\beta_1(\Omega)=\beta_2(\Omega)=0$, and a multiply connected region is one that is not simply connected.

Remark 2: In fact, in order to ensure the uniqueness of (14), the additional condition

$$\int_{\Gamma_i}\boldsymbol{n}\cdot\boldsymbol{\theta}_i\big|^+\,d\boldsymbol{\xi}=0 \tag{18}$$

where Γ_i, $i=1,\cdots,m$ and m denotes the number of closed surfaces making up Γ, should be added. Analogous conditions should be added for systems (16) and (17).

Lemma 3: The tensor $\mathcal{N}^0$ reduces to $\mathcal{T}(\mu_r)$ independently of the geometric configuration of B, and in particular, independently of the first Betti number of B and B^c.

Proof: We introduce $\boldsymbol{v}_i:=\nabla\times\boldsymbol{\theta}_i^{(0)}$ and set $\boldsymbol{u}_i=\tilde{\mu}_r^{-1}\boldsymbol{v}_i$ with $\tilde{\mu}_r:=\begin{cases}\mu_r & \text{in } B\\ 1 & \text{in } B^c\end{cases}$. In doing so, we can establish, using the decay conditions of $\nabla\times\boldsymbol{\theta}_i=O(|\boldsymbol{\xi}|^{-3})$ as $|\boldsymbol{\xi}|\to\infty$ [2], that $\boldsymbol{u}_i$ satisfies the transmission problem

$$\begin{aligned}\nabla\times\boldsymbol{u}_i&=\mathbf{0}\quad\text{in } B\cup B^c &(19a)\\ \nabla\cdot(\tilde{\mu}_r\boldsymbol{u}_i)&=0\quad\text{in } B\cup B^c &(19b)\\ \big[\hat{\boldsymbol{n}}\times\boldsymbol{u}_i\big]_\Gamma&=\mathbf{0}\quad\text{on }\Gamma &(19c)\\ \big[\hat{\boldsymbol{n}}\cdot(\tilde{\mu}_r\boldsymbol{u}_i)\big]_\Gamma&=0\quad\text{on }\Gamma &(19d)\\ \boldsymbol{u}_i(\boldsymbol{\xi})-2\hat{\boldsymbol{e}}_i&=O(|\boldsymbol{\xi}|^{-3})\quad\text{as } |\boldsymbol{\xi}|\to\infty &(19e)\end{aligned}$$

which is equivalent to (16). We set the harmonic fields as $\boldsymbol{u}_i=\nabla\vartheta_i+\boldsymbol{h}_i$ in B and B^c, where $\boldsymbol{h}_i$ represents the curl free fields that are not gradients with $\dim(\boldsymbol{h}_i)=\beta_1(B)$ in B and $\dim(\boldsymbol{h}_i)=\beta_1(B^c)$ in B^c. But, due to the fact that $\boldsymbol{u}_i$ is curl free for all of $\mathbb{R}^3$ in (19), we have, independent of the choice of loops $\gamma_i(B)$, $\gamma_j(B^c)$, that

$$\oint_{\gamma_i(B)}\hat{\boldsymbol{\tau}}\cdot\boldsymbol{u}_i d\boldsymbol{\xi}=\oint_{\gamma_j(B^c)}\hat{\boldsymbol{\tau}}\cdot\boldsymbol{u}_i d\boldsymbol{\xi}=0$$

$i=1,\cdots,\beta_1(B)$, $j=1,\cdots,\beta_1(B^c)$, where $\hat{\boldsymbol{\tau}}$ denotes the unit tangent, and thus, by [11, Proposition 3 and Remark 3], $\boldsymbol{h}_i=\mathbf{0}$ in $\mathbb{R}^3$. Furthermore, by choosing $\vartheta_i:=2(\mu_r-1)\phi_i+2\xi_i$ then (19) reduces to (10) and

$$\begin{aligned}\mathcal{N}_{ij}^0&=\alpha^3(\mu_r-1)\int_B(\hat{\boldsymbol{e}}_i\cdot((\mu_r-1)\nabla\phi_j+\hat{\boldsymbol{e}}_j))d\boldsymbol{\xi}\\ &=\alpha^3\left((\mu_r-1)|B|\delta_{ij}+(\mu_r-1)^2\int_B\hat{\boldsymbol{e}}_i\cdot\nabla\phi_j d\boldsymbol{\xi}\right)\\ &=\alpha^3\left((\mu_r-1)|B|\delta_{ij}+(\mu_r-1)^2\int_\Gamma\hat{\boldsymbol{n}}^-\cdot\nabla\phi_j\xi_i d\boldsymbol{\xi}\right)\end{aligned}$$

where the last step follows by integration points. Finally, we get $\mathcal{N}^0=\mathcal{T}(\mu_r)$ by the symmetry of the coefficients of the tensor [13]. ■

Remark 4: By using the alternative splitting $\overset{\approx}{\mathcal{M}}=\mathcal{N}^{\sigma*}-\check{\mathcal{C}}^{\sigma*}+\mathcal{N}^0$ and Lemma 3, we can now write $\overset{\approx}{\mathcal{M}}=\mathcal{N}^{\sigma*}-\check{\mathcal{C}}^{\sigma*}+\mathcal{T}(\mu_r)$, whereas the original splitting would requires $\sigma_*=0$ for $\overset{\approx}{\mathcal{M}}=\mathcal{N}=\mathcal{T}(\mu_r)$. Thus, the alternative splitting of $\overset{\approx}{\mathcal{M}}$ is useful as it allows us to separate the complex symmetric conducting part $\mathcal{N}^{\sigma*}-\check{\mathcal{C}}^{\sigma*}$ from the real symmetric magnetic part $\mathcal{N}^0=\mathcal{T}(\mu_r)$ and associate the latter with the Pólya–Szegö tensor. We summarize the interrelationships between the different rank 2 tensors in Fig. 2 and emphasize that (12) provides a unified description of $(\boldsymbol{H}_\alpha-\boldsymbol{H}_0)(\boldsymbol{x})$ for eddy current and magnetostatic problems as the object

This article has been accepted for publication in a future issue of this journal, but has not been fully edited. Content may change prior to final publication. Citation information: DOI 10.1109/TMAG.2015.2507169, IEEE Transactions on Magnetics

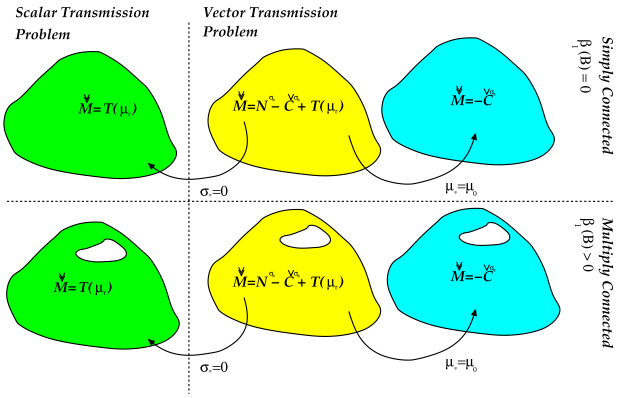

Fig. 2. Family of rank 2 polarization tensors for describing magnetic and conducting, simply and multiply connected, objects.

size tends to zero for both simply connected and multiply connected objects.

Corollary 5: If the background magnetic field $\boldsymbol{H}_0(\boldsymbol{z})$ is assumed to be that produced by a magnetic dipole, such as is appropriate for its evaluation at points away from a current source of small diameter centered at $\boldsymbol{y}$, then it follows that, at the center of the object:

$$(\boldsymbol{H}_0^e)_i := (\boldsymbol{H}_0(\boldsymbol{z}))_i = (\boldsymbol{D}^2 G(\boldsymbol{y},\boldsymbol{z})\boldsymbol{m}^e)_i$$

where $\boldsymbol{m}^e$ is the magnetic dipole moment of exciting current source. Taking the component of (12) in the direction $\boldsymbol{m}^m$ for this background field gives

$$\boldsymbol{m}^m \cdot (\boldsymbol{H}_\alpha - \boldsymbol{H}_0)(\boldsymbol{x}) = \boldsymbol{H}_0^m \cdot (\overset{\approx}{\mathcal{M}}\boldsymbol{H}_0^e) + O(\alpha^4) \qquad (20)$$

as $\alpha \to 0$, where $\boldsymbol{H}_0^m := \boldsymbol{D}^2 G(\boldsymbol{x},\boldsymbol{z})\boldsymbol{m}^m$ is the background magnetic field, evaluated at the center of the object, that would result from considering the measurement coil centered at $\boldsymbol{x}$ to be an excitor with dipole moment $\boldsymbol{m}^m$. We observe that the leading-order term is exactly of the form quoted in (1), and moreover, by applying the Lorentz reciprocity theorem, it is possible to show that this is the leading term in the induced voltage (see the Appendix).

IV. Bounds on the Tensor Coefficients and Associated Properties

A. Preliminaries

Following the restriction to orthonormal coordinates, we will, henceforth, arrange the coefficients of the rank 2 tensors $\mathcal{T}(\mu_r)$ and $\overset{\approx}{\mathcal{M}}$ [and its components $\mathcal{N}^0 = \mathcal{T}(\mu_r)$, $\mathcal{N}^{\sigma *}$, and $\check{\mathcal{C}}^{\sigma *}$] in the form of 3×3 matrices. As standard, we shall compute their eigenvalues and eigenvectors of the tensors by computing the corresponding quantities for their matrix arrangements.

For some real contrast k, we recall that the Pólya–Szegö tensor $\mathcal{T}(k)$ is real symmetric with real eigenvalues and its eigenvectors are mutually perpendicular [4]. It can be diagonalized as

$$(\mathcal{R}^T(\mathcal{T}\mathcal{R}))_{ij} = \mathcal{R}_{ki}\mathcal{T}_{k\ell}\mathcal{R}_{\ell j} = \Lambda_{ij} \qquad (21a)$$

$$\mathcal{T}_{ij} = \mathcal{R}_{ik}\Lambda_{k\ell}\mathcal{R}_{j\ell} = (\mathcal{R}(\Lambda\mathcal{R}^T))_{ij} \qquad (21b)$$

where $\mathcal{R}$ is the real and orthogonal ($\mathcal{R}^{-1} = \mathcal{R}^T$) and whose columns are the tensor's eigenvectors. Furthermore, Λ is diagonal with its enteries λ_1, λ_2, and λ_3 being the eigenvalues of $\mathcal{T}$ (being positive definite for $1 < k < \infty$ and negative definite for $0 < k < 1$).

On the otherhand, as $\overset{\approx}{\mathcal{M}}$ is complex symmetric then, in general, it is not diagonalizable by a real rotation matrix apart for the specific case, where the real and imaginary parts $\overset{\approx}{\mathcal{M}}$ commute, such that $\overset{\approx}{\mathcal{M}} = \overset{\approx}{\mathcal{M}}_r + \mathrm{i}\overset{\approx}{\mathcal{M}}_r$ and in this case

$$(\mathcal{R}^T(\overset{\approx}{\mathcal{M}}\mathcal{R}))_{ij} = \mathcal{R}_{ki}(\overset{\approx}{\mathcal{M}}_r + \mathrm{i}\overset{\approx}{\mathcal{M}}_r)_{k\ell}\mathcal{R}_{\ell j} = \Lambda_{ij} + \mathrm{i}\Lambda_{ij} \qquad (22a)$$

$$\begin{aligned}\overset{\approx}{\mathcal{M}}_{ij} &= \mathcal{R}_{ik}(\Lambda_{k\ell} + \mathrm{i}\Lambda_{k\ell})\mathcal{R}_{j\ell} \\ &= (\mathcal{R}((\Lambda + \mathrm{i}\Lambda)\mathcal{R}^T))_{ij}\end{aligned} \qquad (22b)$$

where the columns of $\mathcal{R}$ are the eigenvectors of $\overset{\approx}{\mathcal{M}}_r$ and Λ is the diagonal with enteries λ_1, λ_2, and λ_3 being the eigenvalues of $\mathcal{M}_r$. The symmetric singular value decomposition [43] can be applied to achieve the diagonalization of a complex symmetric matrix using a unitary matrix, although it remains to be shown whether this decomposition provides any practical insights.

We recall the Cayley–Hamilton theorem, which states that for a symmetric rank 2 tensor $\mathcal{A}$ that

$$\mathcal{A}^3 - I_1\mathcal{A}^2 + I_2\mathcal{A} - I_3\mathcal{I} = 0 \qquad (23)$$

where its invariants are $I_1 = \mathrm{tr}\,(\mathcal{A})$, $I_2 = \frac{1}{2}(I_1^2 - \mathrm{tr}\,(\mathcal{A}\mathcal{A}))$, and $I_3 = \det\mathcal{A}$ and $\mathcal{I}_{ij} = \delta_{ij}$.

B. Some Properties of the Pólya–Szegö Tensor $\mathcal{T}(k)$

We first list some known properties of the Pólya–Szegö tensor $\mathcal{T}(k)$ for $0 < k \neq 1 < \infty$, which by Lemma 3, also carry over to $\mathcal{N}^0$.

1) Kleinman and Senior [26] show that the coefficients of the tensor satisfy

$$\left(\mathcal{T}_{ij} - \frac{k-1}{k+1}|B|\delta_{ij}\alpha^3\right)^2 \leqslant \left(\mathcal{T}_{ii} - \frac{k-1}{k+1}|B|\alpha^3\right)\left(\mathcal{T}_{jj} - \frac{k-1}{k+1}|B|\alpha^3\right) \qquad (24)$$

which is trivially satisfied for the diagonal entries. An alternative proof can be found in [4].

2) Kleinman and Senior [26] also show that the diagonal coefficients of the tensor satisfy

$$\frac{k-1}{k} \leqslant \frac{\mathcal{T}_{ii}}{\alpha^3|B|} \leqslant k-1. \qquad (25)$$

Again, an alternative proof can be found in [4], which also states that the eigenvalues of $\mathcal{T}$ satisfy the same inequality

$$\frac{k-1}{k} \leqslant \frac{\lambda_i(\mathcal{T})}{\alpha^3|B|} \leqslant k-1. \qquad (26)$$

3) The bound on the trace of $\mathcal{T}$, which follows from (25), is not optimum and instead [4] proves the improved result, which we state for three dimensions:

$$\frac{1}{k-1}\mathrm{tr}(\mathcal{T}) \leqslant \left(2+\frac{1}{k}\right)\alpha^3|B| \tag{27}$$

$$(k-1)\mathrm{tr}(\mathcal{T}^{-1}) \leqslant \frac{2+k}{|B|\alpha^3} \tag{28}$$

and has previously been proved in [12].

Using these results, we establish the following.

Lemma 6: For a contrast $1 < k < \infty$, the invariants I_1, I_2, and I_3 of the Pólya–Szegö tensor $\mathcal{T}(k)$ satisfy

$$0 < I_1 \leqslant \left(2+\frac{1}{k}\right)(k-1)\alpha^3|B| \tag{29}$$

$$0 < |I_2| \leqslant \frac{1}{2}\left(7+\frac{4}{k}+\frac{1}{k^2}\right)(k-1)^2\alpha^6|B|^2 \tag{30}$$

$$0 < \alpha^9|B|^3\left(1-\frac{1}{k}\right)^3 \leqslant I_3 \leqslant (k-1)^3\alpha^9|B|^3 \tag{31}$$

in three dimensions. On the other hand, if $0 < k < 1$, then the following inequalities hold:

$$0 > I_1 \geqslant \left(2+\frac{1}{k}\right)(k-1)\alpha^3|B| \tag{32}$$

$$0 < |I_2| \leqslant \frac{1}{2}\left(7+\frac{4}{k}+\frac{1}{k^2}\right)(k-1)^2\alpha^6|B|^2 \tag{33}$$

$$\alpha^9|B|^3\left(1-\frac{1}{k}\right)^3 \leqslant I_3 \leqslant (k-1)^3\alpha^9|B|^3 < 0. \tag{34}$$

Proof: The results (29) and (32) immediately follow from (27).

From (29), $I_1^2 = (\mathrm{tr}(\mathcal{T}))^2 \leqslant \left(2+\frac{1}{k}\right)^2(k-1)^2\alpha^6|B|^2$ for $0 < k \neq 1 < \infty$ and recalling (21b), then $\mathrm{tr}(\mathcal{T}\mathcal{T}) = \mathrm{tr}(\mathcal{R}\Lambda\Lambda\mathcal{R}^T) = \lambda_1^2+\lambda_2^2+\lambda_3^2$. Thus, since $|I_2| = \frac{1}{2}|I_1^2 - (\mathrm{tr}(\mathcal{T}))^2| \leqslant \frac{1}{2}(I_1^2+(\mathrm{tr}(\mathcal{T}))^2)$ and using (26), the results stated in (30) and (33) immediately follow.

Recalling $I_3 = \det(\mathcal{T}) = \lambda_1\lambda_2\lambda_3$ and that $\mathcal{T}$ is positive definite for $1 < k < \infty$ and negative definitive for $0 < k < 1$, then (31) and (34) follow immediately from the substitution of (26). ∎

Corollary 7: It immediately follows from Lemma 6 that the volumetric (spherical) part of $\mathcal{T}$ can be bounded as:

$$3|B|^2\alpha^6\left(\frac{k-1}{k}\right)^2 \leqslant \|\mathrm{diag}(\mathcal{T})\|_F \leqslant 3|B|^2\alpha^6(k-1)^2 \tag{35}$$

where $\|\mathcal{A}\|_F := \left(\sum_{i=1}^3\sum_{j=1}^3|\mathcal{A}_{ij}|^2\right)^{1/2}$ denotes the Forbenius matrix norm.

Lemma 8: The deviatoric part of $\mathcal{T}(k)$ can be bounded as

$$\left\|\mathcal{T}-\frac{1}{3}\mathrm{tr}(\mathcal{T})\right\|_F^2 \leqslant \alpha^6|B|^2(k-1)^2 \times\left(3+\frac{1}{3}\left(2+\frac{1}{k}\right)^2+6\left(1-\frac{1}{k+1}\right)^2\right) \quad \text{if } 1 < k < \infty \tag{36a}$$

and as

$$\left\|\mathcal{T}-\frac{1}{3}\mathrm{tr}(\mathcal{T})\right\|_F^2 \leqslant \alpha^6|B|^2(k-1)^2 \times\left(\frac{3}{k^2}+\frac{1}{3}\left(2+\frac{1}{k}\right)^2+6\left(\frac{1}{k}+\frac{1}{k+1}\right)^2\right) \quad \text{if } 0 < k < 1. \tag{36b}$$

Proof: We consider the case of $1 < k < \infty$, the proof for $0 < k < 1$ is analogous. To show this, we first fix $i = j$ then, by the triangular inequality, (25), and (27), it follows that:

$$\left(\mathcal{T}_{ii}-\frac{1}{3}\mathrm{tr}(\mathcal{T})\right)^2 \leqslant \mathcal{T}_{ii}^2+\frac{1}{9}\mathrm{tr}(\mathcal{T})^2 \leqslant \alpha^6|B|^2(k-1)^2\left(1+\frac{1}{9}\left(2+\frac{1}{k}\right)^2\right). \tag{37}$$

On the other hand, for $i \neq j$, (24) implies that

$$\mathcal{T}_{ij}^2 = \left(\mathcal{T}_{ij}-\frac{1}{3}\mathrm{tr}(\mathcal{T})\delta_{ij}\right)^2 \leqslant \left(\mathcal{T}_{ii}-\alpha^3|B|\left(\frac{k-1}{k+1}\right)\right) \times\left(\mathcal{T}_{jj}-\alpha^3|B|\left(\frac{k-1}{k+1}\right)\right) \leqslant \alpha^6|B|^2(k-1)^2\left(1-\frac{1}{k+1}\right)^2 \tag{38}$$

by the application of (25). Summing (37) over the diagonal entries and (38) over the off-diagonal entries completes the proof. ∎

V. Limiting Low-Frequency and High-Conductivity Responses

In this section, we consider the low-frequency and high-conductivity limiting cases of $\overset{\approx}{\mathcal{M}}$. We also discuss the cases of high frequency and low conductivity. From the results presented in this section, we cannot necessarily deduce the behavior of $(\boldsymbol{H}_\alpha-\boldsymbol{H}_0)(\boldsymbol{x})$ from (12), since it is not permitted to substitute one asymptotic expansion, where $\alpha \to 0$ (and ω and σ_* are fixed through ν), into another, where α is fixed and different limits on ω and σ_* are taken. Still further, the eddy-current model represents a quasi-static approximation to the Maxwell system, and in order that the modeling error is small, ω and σ_* should be chosen according to shape-dependent constants [39]. Nonetheless, our theoretical results do have great practical relevence as the examples in Sections VI–VIII illustrate. We first consider the low-frequency response followed by the high-conductivity case.

Theorem 9: The low-frequency limit for the coefficients of $\overset{\approx}{\mathcal{M}}$ can be described as

$$\overset{\approx}{\mathcal{M}}_{ij} = \mathcal{N}_{ij}^0(\mu_r)+O(\omega) = \mathcal{T}_{ij}(\mu_r)+O(\omega) \tag{39}$$

as $\omega \to 0$ for an object B with fixed conductivity σ_* and relative permeability μ_r.

Proof: We recall the splittiing $\boldsymbol{\theta}_i = \boldsymbol{\theta}_i^{(0)}+\boldsymbol{\theta}_i^{(1)}-\hat{\boldsymbol{e}}_i\times\boldsymbol{\xi}$ and that $\boldsymbol{\theta}_i^{(0)}$ and $\boldsymbol{\theta}_i^{(1)}$ solve (16) and (17), respectively. The weak

form of the transmission problem for $\boldsymbol{\theta}_i^{(1)}$ is: find $\boldsymbol{\theta}_i^{(1)} \in X$, such that

$$\int_\Omega \nabla \times \boldsymbol{\theta}_i^{(1)} \cdot \nabla \times \boldsymbol{w} - \mathrm{i}\omega\sigma\,\mu\alpha^2 \boldsymbol{\theta}_i^{(1)} \cdot \boldsymbol{w} d\boldsymbol{\xi} = \mathrm{i}\omega\sigma_*\mu_*\alpha^2 \int_B \boldsymbol{\theta}_i^{(0)} \cdot \boldsymbol{w} d\boldsymbol{\xi} \quad \forall \boldsymbol{w} \in X \quad (40)$$

where $X := \{\boldsymbol{u} \in \boldsymbol{H}(\mathrm{curl}(\Omega)) : \nabla \cdot \boldsymbol{u} = 0 \text{ in } \Omega\}$ and $\Omega = B^c \cup B$. Note that we have extended the requirement that $\boldsymbol{\theta}_i^{(1)}$ be divergence free from B^c to Ω, but this is an immediate consequence of (17a). Choosing $\boldsymbol{w} = (\boldsymbol{\theta}_i^{(1)})^*$ in (40), where $*$ denotes the complex conjugate, it follows for fixed α, μ_*, and σ_* that:

$$\begin{aligned}
\|\nabla \times \boldsymbol{\theta}_i^{(1)}\|_{L^2(\Omega)}^2 &= \int_\Omega |\nabla \times \boldsymbol{\theta}_i^{(1)}|^2 d\boldsymbol{\xi} \\
&\leqslant \left| \int_\Omega |\nabla \times \boldsymbol{\theta}_i^{(1)}|^2 - \mathrm{i}\omega\sigma\,\mu\alpha^2 |\boldsymbol{\theta}_i^{(1)}|^2 d\boldsymbol{\xi} \right| \\
&= \omega\sigma_*\mu_*\alpha^2 \left| \int_B \boldsymbol{\theta}_i^{(0)} \cdot \left(\boldsymbol{\theta}_i^{(1)}\right)^* d\boldsymbol{\xi} \right| \\
&\leqslant C\omega \|\boldsymbol{\theta}_i^{(0)}\|_{L^2(B)} \|\boldsymbol{\theta}_i^{(1)}\|_{L^2(B)} \\
&\leqslant C\omega \|\boldsymbol{\theta}_i^{(1)}\|_{L^2(\Omega)}
\end{aligned}$$

where C is a generic constant independent of ω and $\boldsymbol{\theta}_i^{(1)}$ and the Cauchy–Schwartz inequality has been applied in the second to last step. Then, by using [33, p. 72, Corollary 3.51] and the far field decay of $\boldsymbol{\theta}_i^{(1)}$, we have $\|\boldsymbol{\theta}_i^{(1)}\|_{L^2(\Omega)} \leqslant C\|\nabla \times \boldsymbol{\theta}_i^{(1)}\|_{L^2(\Omega)}$, so that

$$\|\nabla \times \boldsymbol{\theta}_i^{(1)}\|_{L^2(B)} \leqslant \|\nabla \times \boldsymbol{\theta}_i^{(1)}\|_{L^2(\Omega)} \leqslant C\omega. \quad (41)$$

We use this result and the Cauchy–Schwartz inequality to establish the following:

$$\begin{aligned}
|\check{\mathcal{C}}_{ij}^{\sigma_*}| &= \frac{\nu\alpha^3}{4} \left| \hat{\boldsymbol{e}}_i \cdot \int_B \boldsymbol{\xi} \times \left(\boldsymbol{\theta}_j^{(0)} + \boldsymbol{\theta}_j^{(1)}\right) d\boldsymbol{\xi} \right| \\
&\leqslant C\omega \left(\left| \int_B \boldsymbol{\theta}_j^{(0)} \cdot \boldsymbol{\xi} \times \hat{\boldsymbol{e}}_i d\boldsymbol{\xi} \right| + \left| \int_B \boldsymbol{\theta}_j^{(1)} \cdot \boldsymbol{\xi} \times \hat{\boldsymbol{e}}_i d\boldsymbol{\xi} \right| \right) \\
&\leqslant C\omega \left(\|\boldsymbol{\theta}_j^{(0)}\|_{L^2(B)} + \|\boldsymbol{\theta}_j^{(1)}\|_{L^2(B)} \right) \\
&\leqslant C\omega \left(1 + \|\boldsymbol{\theta}_j^{(1)}\|_{L^2(B)}\right) \quad (42) \\
|\mathcal{N}_{ij}^{\sigma_*}| &= \left| \frac{\alpha^3}{2} \left(1 - \frac{\mu_0}{\mu_*}\right) \int_B \left(\hat{\boldsymbol{e}}_i \cdot \nabla \times \boldsymbol{\theta}_j^{(1)}\right) d\boldsymbol{\xi} \right| \\
&\leqslant C\|\nabla \times \boldsymbol{\theta}_j^{(1)}\|_{L^2(B)} \leqslant C\omega \quad (43) \\
|\mathcal{N}_{ij}^{0}| &= \left| \frac{\alpha^3}{2} \left(1 - \frac{\mu_0}{\mu_*}\right) \int_B \left(\hat{\boldsymbol{e}}_i \cdot \nabla \times \boldsymbol{\theta}_j^{(0)}\right) d\boldsymbol{\xi} \right| \\
&\leqslant C\|\nabla \times \boldsymbol{\theta}_j^{(0)}\|_{L^2(B)} \leqslant C. \quad (44)
\end{aligned}$$

Combining (42)–(44) and using the decomposition $\overset{\approx}{\mathcal{M}}_{ij} = -\check{\mathcal{C}}_{ij}^{\sigma_*} + \mathcal{N}_{ij}^{\sigma_*} + \mathcal{N}_{ij}^{0}$, the desired result immediately follows. The reduction to $\mathcal{T}_{ij}$ follows immediately from Lemma 3. ■

Remark 10: By following analogous steps, one can also establish that $\overset{\approx}{\mathcal{M}}_{ij} = T(\mu_r) + O(\sigma_*)$ as $\sigma_* \to 0$ for an object B with fixed relative permeability μ_r and frequency ω. However, further to the comments at the beginning of this section, one needs to be careful with the applicability of such a result.

Theorem 11: The high conductivity limit of the coefficients of $\overset{\approx}{\mathcal{M}}$ can be described as

$$\overset{\approx}{\mathcal{M}}_{ij} = \mathcal{T}_{ij}(0) + O\left(\frac{1}{\sqrt{\sigma_*}}\right) \quad (45)$$

as $\sigma_* \to \infty$ for a object B, with $\beta_1(B) = \beta_1(B^c) = 0$, fixed frequency ω, and relative permeability μ_r. Specifically

$$\mathcal{T}_{ij}(0) = \alpha^3 \left(|B|\delta_{ij} - \int_\Gamma \hat{\boldsymbol{n}}^- \cdot \hat{\boldsymbol{e}}_i \psi_j d\boldsymbol{\xi} \right) \quad (46)$$

and ψ_j solves

$$\begin{aligned}
\nabla^2 \psi_j &= 0 \quad \text{in } B^c && (47a) \\
\hat{\boldsymbol{n}} \cdot \nabla \psi_j &= \hat{\boldsymbol{n}} \cdot \nabla \xi_j \quad \text{on } \Gamma && (47b) \\
\psi_j &\to 0 \quad \text{as } |\boldsymbol{\xi}| \to \infty. && (47c)
\end{aligned}$$

Before proving this result, we first consider the following intermediate lemma.

Lemma 12: The coefficients of $\overset{\approx}{\mathcal{M}}$ can be expressed as

$$\begin{aligned}
\overset{\approx}{\mathcal{M}}_{ij} &= \frac{\alpha^3}{2} \int_\Gamma \hat{\boldsymbol{e}}_i \cdot \boldsymbol{\theta}_j \times \hat{\boldsymbol{n}}^+|_+ d\boldsymbol{\xi} \\
&\quad - \frac{\alpha^3}{4} \int_\Gamma \hat{\boldsymbol{e}}_i \times \boldsymbol{\xi} \cdot \hat{\boldsymbol{n}}^+ \times \nabla \times \boldsymbol{\theta}_j|_+ d\boldsymbol{\xi}. \quad (48)
\end{aligned}$$

Proof: We begin by expressing $\check{\mathcal{C}}_{ij}$ in an alternative form

$$\begin{aligned}
\check{\mathcal{C}}_{ij} &= -\frac{\mathrm{i}\nu\alpha^3}{4} \hat{\boldsymbol{e}}_i \cdot \int_B \boldsymbol{\xi} \times (\boldsymbol{\theta}_j + \hat{\boldsymbol{e}}_j \times \boldsymbol{\xi}) d\boldsymbol{\xi} \\
&= -\frac{\alpha^3}{4\mu_r} \int_B \nabla \times \nabla \times \boldsymbol{\theta}_j \cdot \hat{\boldsymbol{e}}_i \times \boldsymbol{\xi} d\boldsymbol{\xi} \\
&= -\frac{\alpha^3}{4} \int_\Gamma \hat{\boldsymbol{e}}_i \times \boldsymbol{\xi} \cdot \hat{\boldsymbol{n}}^- \times \mu_r^{-1} \nabla \times \boldsymbol{\theta}_j|_- d\boldsymbol{\xi} \\
&\quad + \frac{\alpha^3}{2\mu_r} \int_\Gamma \hat{\boldsymbol{e}}_i \cdot \boldsymbol{\theta}_j \times \hat{\boldsymbol{n}}^-|_- d\boldsymbol{\xi}
\end{aligned}$$

which follows from using $\boldsymbol{\theta}_j + \hat{\boldsymbol{e}}_j \times \boldsymbol{\xi} = (1/\mathrm{i}\nu\mu_r)\nabla \times \nabla \times \boldsymbol{\theta}_j$ in B and performing integration by parts. Then, by using the transmission conditions for $\boldsymbol{\theta}_j$

$$\begin{aligned}
\check{\mathcal{C}}_{ij} &= -\frac{\alpha^3}{4} \int_\Gamma \hat{\boldsymbol{e}}_i \times \boldsymbol{\xi} \cdot \left(\hat{\boldsymbol{n}}^- \times \nabla \times \boldsymbol{\theta}_j|_+ + 2\left(1 - \mu_r^{-1}\right)\hat{\boldsymbol{n}}^- \right. \\
&\qquad \left. \times \hat{\boldsymbol{e}}_j\right) d\boldsymbol{\xi} - \frac{\alpha^3}{2\mu_r} \int_\Gamma \hat{\boldsymbol{e}}_i \cdot \boldsymbol{\theta}_j \times \hat{\boldsymbol{n}}^+|_+ d\boldsymbol{\xi}.
\end{aligned}$$

On the other hand

$$\begin{aligned}
\mathcal{N}_{ij} &= \alpha^3 \left(1 - \mu_r^{-1}\right) \int_B \left(\delta_{ij} + \frac{1}{2} \hat{\boldsymbol{e}}_i \cdot \nabla \times \boldsymbol{\theta}_j\right) d\boldsymbol{\xi} \\
&= \alpha^3 \left(1 - \mu_r^{-1}\right) \left(|B|\delta_{ij} + \frac{1}{2} \int \hat{\boldsymbol{e}}_i \cdot \boldsymbol{\theta}_j \times \hat{\boldsymbol{n}}^+|_+ d\boldsymbol{\xi} \right)
\end{aligned}$$

by integration by parts and application of a transmission condition. By realizing that

$$\frac{\alpha^3}{2}\left(1 - \mu_r^{-1}\right) \int_\Gamma \hat{\boldsymbol{e}}_i \times \boldsymbol{\xi} \cdot \hat{\boldsymbol{n}}^- \times \hat{\boldsymbol{e}}_j d\boldsymbol{\xi} = -\alpha^3 |B| \left(1 - \mu_r^{-1}\right) \delta_{ij}$$

it follows:

$$\widetilde{\widetilde{\mathcal{M}}}_{ij} = -\check{\mathcal{C}}_{ij} + \mathcal{N}_{ij} = \frac{\alpha^3}{2}\int_\Gamma \hat{\boldsymbol{e}}_i \cdot \boldsymbol{\theta}_j \times \hat{\boldsymbol{n}}^+|_+ d\boldsymbol{\xi} + \frac{\alpha^3}{4}\int_\Gamma \hat{\boldsymbol{e}}_i \times \boldsymbol{\xi} \cdot \hat{\boldsymbol{n}}^- \times \nabla \times \boldsymbol{\theta}_j|_+ d\boldsymbol{\xi}$$

from which immediately follows the desired result. ∎

Proof of Theorem 11: Consider the decomposition $\boldsymbol{\theta}_i = \boldsymbol{\Delta}_i + \begin{cases} \boldsymbol{\chi}_i & \text{in } B^c \\ \boldsymbol{\psi}_i & \text{in } B \end{cases}$, where

$$\nabla \times \mu_0^{-1} \nabla \times \boldsymbol{\chi}_i = \boldsymbol{0} \quad \text{in } B^c \tag{49a}$$
$$\nabla \cdot \boldsymbol{\chi}_i = 0 \quad \text{in } B^c \tag{49b}$$
$$\nabla \times \boldsymbol{\chi}_i \times \hat{\boldsymbol{n}} = -2\hat{\boldsymbol{e}}_i \times \hat{\boldsymbol{n}} \quad \text{on } \Gamma \tag{49c}$$
$$\boldsymbol{\chi}_i(\boldsymbol{\xi}) = O(|\boldsymbol{\xi}|^{-1}) \quad \text{as } |\boldsymbol{\xi}| \to \infty \tag{49d}$$

and

$$\nabla \times \mu_*^{-1} \nabla \times \boldsymbol{\psi}_i - \mathrm{i}\omega\sigma_*\alpha^2\boldsymbol{\psi}_i = \mathrm{i}\omega\sigma_*\alpha^2\boldsymbol{e}_i \times \boldsymbol{\xi} \quad \text{in } B \tag{50a}$$
$$\nabla \cdot \boldsymbol{\psi}_i = 0 \quad \text{in } B \tag{50b}$$
$$\nabla \times \boldsymbol{\psi}_i \times \hat{\boldsymbol{n}} = -2\hat{\boldsymbol{e}}_i \times \hat{\boldsymbol{n}} + \frac{\mu_*}{\nu\mu_0}\nabla \times \boldsymbol{\chi}_i \times \hat{\boldsymbol{n}}|_+ \quad \text{on } \Gamma \tag{50c}$$

such that the problems inside and outside the object completely decouple in the case of high conductivity, since $\nu = \alpha^2\omega\sigma_*\mu_0$. The transmission problem for $\boldsymbol{\Delta}_i$ is

$$\nabla \times \mu^{-1} \nabla \times \boldsymbol{\Delta}_i - \mathrm{i}\omega\sigma\alpha^2\boldsymbol{\Delta}_i = \boldsymbol{0} \quad \text{in } B \cup B^c \tag{51a}$$
$$\nabla \cdot \boldsymbol{\Delta}_i = 0 \quad \text{in } B \cup B^c \tag{51b}$$
$$[\boldsymbol{\Delta}_i \times \hat{\boldsymbol{n}}]_\Gamma = \boldsymbol{0} \quad \text{on } \Gamma \tag{51c}$$
$$[\mu^{-1}\nabla \times \boldsymbol{\Delta}_i \times \hat{\boldsymbol{n}}]_\Gamma = \frac{1}{\nu\mu_0}\nabla \times \boldsymbol{\chi}_i \times \hat{\boldsymbol{n}} \quad \text{on } \Gamma \tag{51d}$$
$$\boldsymbol{\Delta}_i(\boldsymbol{\xi}) = O(|\boldsymbol{\xi}|^{-1}) \quad \text{as } |\boldsymbol{\xi}| \to \infty. \tag{51e}$$

In a similar manner to the proof of Lemma 3, we introduce $\boldsymbol{u}_i := \nabla \times \boldsymbol{\chi}_i$ but, in this case, we have only $\boldsymbol{u}_i = 2(s-1)\nabla\vartheta_i + \boldsymbol{h}_i$ in B^c rather than $\mathbb{R}^3$, for some parameter s where $\dim(\boldsymbol{h}_i) = \beta_1(B^c)$, and thus, we can no longer establish that $\boldsymbol{h}_i = \boldsymbol{0}$ independent of the topology of B and B^c. Therefore, we restrict ourselves to the situation of an object, such that $\beta_1(B) = \beta_1(B^c) = 0$, and in this case, $\boldsymbol{u}_i = 2(s-1)\nabla\vartheta_i$, where ϑ_i is the solution to

$$\nabla^2\vartheta_i = 0 \quad \text{in } B^c \tag{52a}$$
$$(s-1)\hat{\boldsymbol{n}} \cdot \nabla\vartheta_i = -\hat{\boldsymbol{n}} \cdot \nabla\xi_i \quad \text{on } \Gamma \tag{52b}$$
$$\vartheta_i \to 0 \quad \text{as } |\boldsymbol{\xi}| \to \infty. \tag{52c}$$

We use the form of $\widetilde{\widetilde{\mathcal{M}}}_{ij}$ established in Lemma 12 and first write $\widetilde{\widetilde{\mathcal{M}}}_{ij} = \widetilde{\widetilde{\mathcal{M}}}^{\chi}_{ij} + \widetilde{\widetilde{\mathcal{M}}}^{\Delta}_{ij}$, where

$$\widetilde{\widetilde{\mathcal{M}}}^{\chi}_{ij} = \frac{\alpha^3}{2}\int_\Gamma \hat{\boldsymbol{e}}_i \cdot \boldsymbol{\chi}_j \times \hat{\boldsymbol{n}}^+|_+ d\boldsymbol{\xi} - \frac{\alpha^3}{4}\int_\Gamma \hat{\boldsymbol{e}}_i \times \boldsymbol{\xi} \cdot \hat{\boldsymbol{n}}^+ \times \nabla \times \boldsymbol{\chi}_j|_+ d\boldsymbol{\xi} \tag{53}$$

$$\widetilde{\widetilde{\mathcal{M}}}^{\Delta}_{ij} = \frac{\alpha^3}{2}\int_\Gamma \hat{\boldsymbol{e}}_i \cdot \boldsymbol{\Delta}_j \times \hat{\boldsymbol{n}}^+|_+ d\boldsymbol{\xi} - \frac{\alpha^3}{4}\int_\Gamma \hat{\boldsymbol{e}}_i \times \boldsymbol{\xi} \cdot \hat{\boldsymbol{n}}^+ \times \nabla \times \boldsymbol{\Delta}_j|_+ d\boldsymbol{\xi}. \tag{54}$$

Considering integration by parts on the first term in (53), we establish that

$$\begin{aligned}
&\frac{\alpha^3}{2}\int_\Gamma \hat{\boldsymbol{e}}_i \cdot \boldsymbol{\chi}_j \times \hat{\boldsymbol{n}}^+|_+ d\boldsymbol{\xi} \\
&= -\frac{\alpha^3}{2}\int_{B^c} \hat{\boldsymbol{e}}_i \cdot \nabla \times \boldsymbol{\chi}_j d\boldsymbol{\xi} \\
&= -\alpha^3(s-1)\int_{B^c} \hat{\boldsymbol{e}}_i \cdot \nabla\vartheta_j d\boldsymbol{\xi} \\
&= -\alpha^3(s-1)\left(\int_{B^c} \hat{\boldsymbol{e}}_i \cdot \nabla\theta_j d\boldsymbol{\xi} + \int_{B^c} \vartheta_j \nabla^2\xi_i d\boldsymbol{\xi}\right) \\
&= -\alpha^3(s-1)\int_\Gamma \hat{\boldsymbol{n}}^+ \cdot \nabla\xi_i\vartheta_j d\boldsymbol{\xi}
\end{aligned} \tag{55}$$

and for the second term, by substituting $\nabla \times \boldsymbol{\chi}_i = 2(s-1)\nabla\vartheta_i$ and using the condition $(s-1)\hat{\boldsymbol{n}} \cdot \nabla\vartheta_i = -\hat{\boldsymbol{n}} \cdot \nabla\xi_i$ on Γ

$$\begin{aligned}
&-\frac{\alpha^3}{4}\int_\Gamma \hat{\boldsymbol{e}}_i \times \boldsymbol{\xi} \cdot \hat{\boldsymbol{n}}^+ \times \nabla \times \boldsymbol{\chi}_j|_+ d\boldsymbol{\xi} \\
&= -\frac{\alpha^3}{2}(s-1)\int_\Gamma \hat{\boldsymbol{n}}^+ \cdot (\nabla\vartheta_j \times (\hat{\boldsymbol{e}}_i \times \boldsymbol{\xi}))d\boldsymbol{\xi} \\
&= \alpha^3(s-1)\int_{B^c} \nabla\vartheta_j \cdot \nabla\xi_i d\boldsymbol{\xi} \\
&= \alpha^3(s-1)\int_\Gamma \hat{\boldsymbol{n}}^+ \cdot \nabla\vartheta_j\xi_i d\boldsymbol{\xi} \\
&= -\alpha^3\int_\Gamma \hat{\boldsymbol{n}}^+ \cdot \nabla\xi_j\xi_i d\boldsymbol{\xi} = \alpha^3|B|\delta_{ij}.
\end{aligned}$$

Adding (55) and (56) for $s = 0$ gives

$$\begin{aligned}
\widetilde{\widetilde{\mathcal{M}}}^{\chi}_{ij} &= \alpha^3|B|\delta_{ij} + \alpha^3\int_\Gamma \hat{\boldsymbol{n}}^+ \cdot \nabla\xi_i\vartheta_j d\boldsymbol{\xi} \\
&= \alpha^3|B|\delta_{ij} - \alpha^3\int_\Gamma \hat{\boldsymbol{n}}^- \cdot \nabla\xi_i\vartheta_j d\boldsymbol{\xi} = \mathcal{T}_{ij}(0)
\end{aligned} \tag{56}$$

where $\mathcal{T}_{ij}(0)$ is as defined in (46) and the problem for ϑ_i becomes that for ψ_i stated in (47). To bound $\widetilde{\widetilde{\mathcal{M}}}^{\Delta}_{ij}$, we consider the weak form of the transmission problem for $\boldsymbol{\Delta}_i$: Find $\boldsymbol{\Delta}_i \in X$, such that

$$\int_\Omega \tilde{\mu}_r^{-1}\nabla \times \boldsymbol{\Delta}_i \cdot \nabla \times \boldsymbol{w} - \mathrm{i}\omega\sigma\mu_0\alpha^2\boldsymbol{\Delta}_i \cdot \boldsymbol{w}d\boldsymbol{\xi} = -\frac{1}{\nu}\int_\Gamma \hat{\boldsymbol{n}} \times \nabla \times \boldsymbol{\chi}_i \cdot \boldsymbol{w}d\boldsymbol{\xi} \quad \forall \boldsymbol{w} \in X. \tag{57}$$

If we choose $\boldsymbol{w} = (\boldsymbol{\Delta}_i)^*$, then it follows for fixed α, μ_*, and ω that:

$$\begin{aligned}
\|\nabla \times \boldsymbol{\Delta}_i\|^2_{L^2(\Omega)} &\leqslant C\left|\int_\Omega \tilde{\mu}_r^{-1}|\nabla \times \boldsymbol{\Delta}_i|^2 - \mathrm{i}\omega\sigma\mu_0\alpha^2|\boldsymbol{\Delta}_i|^2 d\boldsymbol{\xi}\right| \\
&\leqslant \frac{C}{\sigma_*}\left|\int_\Gamma \hat{\boldsymbol{n}}^+ \times \nabla \times \boldsymbol{\chi}_i \cdot (\boldsymbol{\Delta}_i)^* d\boldsymbol{\xi}\right| \\
&\leqslant \frac{C}{\sigma_*}\left|\int_{B^c} \nabla \times \boldsymbol{\chi}_i \cdot (\nabla \times \boldsymbol{\Delta}_i)^* d\boldsymbol{\xi}\right| \\
&\leqslant \frac{C}{\sigma_*}\|\nabla \times \boldsymbol{\chi}_i\|_{L^2(B^c)}\|\nabla \times \boldsymbol{\Delta}_i\|_{L^2(B^c)} \\
&\leqslant \frac{C}{\sigma_*}\|\nabla \times \boldsymbol{\Delta}_i\|_{L^2(\Omega)}
\end{aligned} \tag{58}$$

This article has been accepted for publication in a future issue of this journal, but has not been fully edited. Content may change prior to final publication. Citation information: DOI 10.1109/TMAG.2015.2507169, IEEE Transactions on Magnetics

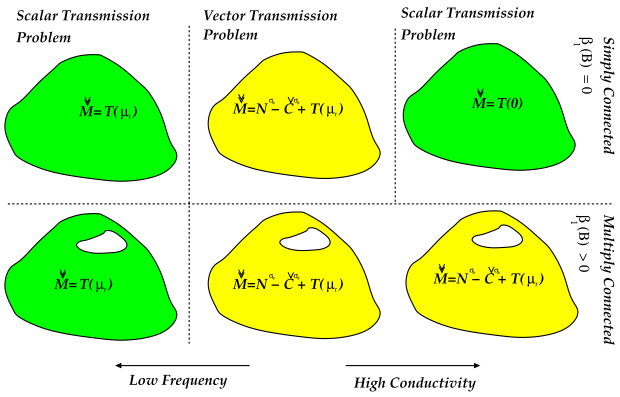

Fig. 3. Limiting cases of low frequency and high conductivity for simply and multiply connected objects.

where integration by parts and then the Cauchy–Schwartz inequality has been applied and C is independent of σ_*. It then follows that:

$$\|\nabla \times \mathbf{\Delta}_i\|_{L^2(B)} \leqslant \frac{C}{\sigma_*} \text{ and } \|\nabla \times \mathbf{\Delta}_i\|_{L^2(B^c)} \leqslant \frac{C}{\sigma_*}.$$

In a similar way, we establish that $\|\mathbf{\Delta}_i\|^2_{L^2(B)} \leqslant (C/\sigma_*)\|\nabla \times \mathbf{\Delta}_i\|_{L^2(\Omega)}$, so that

$$\|\mathbf{\Delta}_i\|_{L^2(B)} \leqslant \frac{C}{\sigma_*^{3/2}}. \tag{59}$$

We then write (54) as

$$\begin{aligned}
\overleftrightarrow{\mathcal{M}}^{\Delta}_{ij} &= -\frac{\alpha^3}{2}\int_{B^c} \hat{\boldsymbol{e}}_i \cdot \nabla \times \mathbf{\Delta}_j d\boldsymbol{\xi} \\
&\quad - \frac{\alpha^3}{4\nu\mu_r}\int_{\Gamma} \hat{\boldsymbol{e}}_i \times \boldsymbol{\xi} \cdot \hat{\boldsymbol{n}}^+ \times \nabla \times \boldsymbol{\chi}_j|_+ d\boldsymbol{\xi} \\
&\quad - \frac{\alpha^3}{4\mu_r}\int_{\Gamma} \hat{\boldsymbol{e}}_i \times \boldsymbol{\xi} \cdot \hat{\boldsymbol{n}}^+ \times \nabla \times \mathbf{\Delta}_j|_- d\boldsymbol{\xi} \\
&= -\frac{\alpha^3}{2}\int_{B^c} \hat{\boldsymbol{e}}_i \cdot \nabla \times \mathbf{\Delta}_j d\boldsymbol{\xi} + \frac{\alpha^3}{2\nu\mu_r}\int_{B^c} \hat{\boldsymbol{e}}_i \cdot \nabla \times \boldsymbol{\chi}_j d\boldsymbol{\xi} \\
&\quad + \frac{\alpha^3}{4}\int_{B} (\mathrm{i}\nu \mathbf{\Delta}_j \cdot \hat{\boldsymbol{e}}_i \times \boldsymbol{\xi} + 2\nabla \times \mathbf{\Delta}_j \cdot \hat{\boldsymbol{e}}_i)\, d\boldsymbol{\xi}.
\end{aligned}$$

Thus, by the Cauchy–Schwartz inequality, it follows that:

$$\begin{aligned}
|\overleftrightarrow{\mathcal{M}}^{\chi}_{ij}| &\leqslant C + C\|\nabla\psi_j\|_{L^2(B^c)} \leqslant C \\
|\overleftrightarrow{\mathcal{M}}^{\Delta}_{ij}| &\leqslant C\|\nabla \times \mathbf{\Delta}_j\|_{L^2(B^c)} + \frac{C}{\sigma_*}\|\nabla \times \boldsymbol{\chi}_j\|_{L^2(B^c)} \\
&\quad + C\sigma_*\|\mathbf{\Delta}_j\|_{L^2(B)} + C\|\nabla \times \mathbf{\Delta}_j\|_{L^2(B)} \\
&\leqslant \frac{C}{\sigma_*} + C\sigma_*\|\mathbf{\Delta}_j\|_{L^2(B)} \leqslant \frac{C}{\sigma_*} + \frac{C}{\sqrt{\sigma_*}} \leqslant \frac{C}{\sqrt{\sigma_*}}
\end{aligned}$$

where C does not depend on σ_* and, consequently, $\overleftrightarrow{\mathcal{M}}_{ij} = \overleftrightarrow{\mathcal{M}}^{\chi}_{ij} + \overleftrightarrow{\mathcal{M}}^{\Delta}_{ij} = \overleftrightarrow{\mathcal{M}}^{\chi}_{ij} + O(1/\sqrt{\sigma_*})$ as $\sigma_* \to \infty$, and consequently, the result stated in (45) directly follows. ■

We summarize our results for the limiting cases of low frequencies and high conductivities in Fig. 3.

Remark 13: We could apply similar arguments and establish that $\overleftrightarrow{\mathcal{M}}_{ij} = \mathcal{T}(0)_{ij} + O(1/\sqrt{\omega})$ as $\omega \to \infty$ for an object with $\beta_1(B) = \beta_1(B^c) = 0$ and fixed relative permeability μ_r and conductivity σ_*. However, similar to Remark 10, we need to be careful with the applicability of such a result. We will return to this point in Section VI.

Remark 14: Noting that the coefficients of the tensors $\mathcal{T}(\mu_r)_{ij}$ and $\mathcal{T}(0)_{ij}$ are real valued, then the behavior obtained at low frequencies, $\overleftrightarrow{\mathcal{M}}_{ij} = \mathcal{T}(\mu_r)_{ij} + O(\omega)$ as $\omega \to 0$, and at high frequencies, $\overleftrightarrow{\mathcal{M}}_{ij} = \mathcal{T}(0)_{ij} + O(1/\sqrt{\omega})$ as $\omega \to \infty$, ties in with the explanation of Landau and Lipshitz [27, pp. 192], who predict that the imaginary component of the magnetic polarizability tensor is proportional to ω as $\omega \to 0$ and is proportional $1/\sqrt{\omega}$ as $\omega \to \infty$ for a simply connected object. Furthermore, they argue that, as $\omega \to \infty$, the magnetic polarizability tensor becomes that of a super conductor. The coefficients $\mathcal{T}(0)_{ij}$ are those of the Póyla–Szegö tensor and are already known to be associated with the magnetic response of a simply connected perfect conductor [29]. A super conductor is the case of a perfect conductor with zero magnetic field in the bulk of the conductor.

VI. Elliptical Objects

For an ellipsoidal object B_α defined as

$$\frac{x_1^2}{a^2} + \frac{x_2^2}{b^2} + \frac{x_3^3}{c^2} = 1, \quad 0 < c \leqslant b \leqslant a$$

and whose principal axes are chosen to coincide with the Cartesian coordinates axes, then an analytical solution is known for the Pólya–Szegö tensor [4]

$$\begin{aligned}
\mathcal{T}(k) &= \frac{4\pi abc}{3} \\
&\times \begin{pmatrix} \dfrac{(k-1)}{(1-A_1)+kA_1} & 0 & 0 \\ 0 & \dfrac{(k-1)}{(1-A_2)+kA_2} & 0 \\ 0 & 0 & \dfrac{(k-1)}{(1-A_3)+kA_3} \end{pmatrix}
\end{aligned}$$

where in the above, the constants A_1, A_2, and A_3 are defined as

$$\begin{aligned}
A_1 &= \frac{bc}{a^2}\int_1^{+\infty} \frac{1}{t^2\sqrt{t^2-1+\left(\frac{b}{a}\right)^2}\sqrt{t^2-1+\left(\frac{c}{a}\right)^2}} dt \\
A_2 &= \frac{bc}{a^2}\int_1^{+\infty} \frac{1}{t^2\left(t^2-1+\left(\frac{b}{a}\right)^2\right)^{3/2}\sqrt{t^2-1+\left(\frac{c}{a}\right)^2}} dt \\
A_3 &= \frac{bc}{a^2}\int_1^{+\infty} \frac{1}{t^2\sqrt{t^2-1+\left(\frac{b}{a}\right)^2}\left(t^2-1+\left(\frac{c}{a}\right)^2\right)^{3/2}} dt
\end{aligned}$$

or by the manipulation of the integrals, A_1, A_2, and A_3 can be expressed as

$$A_1 = \frac{abc}{2}d_1, \quad A_2 = \frac{abc}{2}d_2, \quad A_3 = \frac{abc}{2}d_3 \tag{60}$$

where d_j, $j = 1, 2, 3$ are the depolarizing/demagnetizing factors as defined in [32, pp. 128]. Alternatively, A_j, $j = 1, 2, 3$ can also be expressed in terms of elliptic integrals [36]. By considering the case where $k = \mu_r \to 0$, the Pólya–Szegö

This article has been accepted for publication in a future issue of this journal, but has not been fully edited. Content may change prior to final publication. Citation information: DOI 10.1109/TMAG.2015.2507169, IEEE Transactions on Magnetics

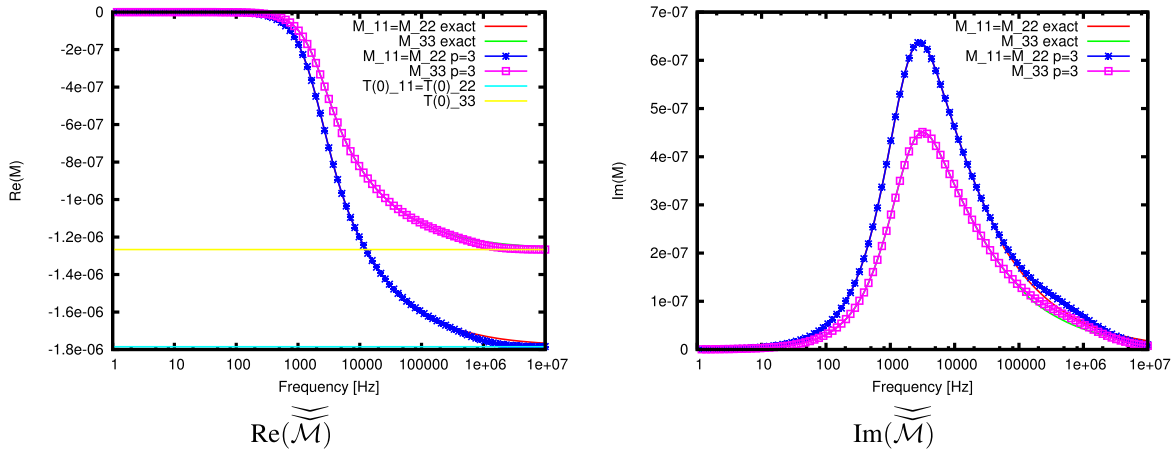

$\mathrm{Re}(\widetilde{\widetilde{\mathcal{M}}})$ $\mathrm{Im}(\widetilde{\widetilde{\mathcal{M}}})$

Fig. 4. Frequency response of a conducting spheroid with $a = 0.02$ m, $b = c = 0.01$ m with $\sigma_* = 1.5 \times 10^7$ S/m, $\mu_* = \mu_0$ showing the diagonal coefficients of $\widetilde{\widetilde{\mathcal{M}}}$ based on the analytical solution in [7], the numerically computed coefficients using the approach of [28] with an unstructured grid of 14 579 tetrahedra and uniform $p = 3$ elements, and the limiting $\mathcal{T}(0)$ coefficients.

tensor $\mathcal{T}(0)$ describes the (magnetic) response for a perfectly conducting object

$$\mathcal{T}(0) = -\frac{4}{3}\pi abc \begin{pmatrix} \dfrac{1}{1-A_1} & 0 & 0 \\ 0 & \dfrac{1}{1-A_2} & 0 \\ 0 & 0 & \dfrac{1}{1-A_3} \end{pmatrix}.$$

Furthermore, on consideration of the diagonalization property of $\mathcal{T}(\mu_r)$ in (21b), and the well known result that $(\boldsymbol{x})_i \Lambda_{ij} (\boldsymbol{x})_j = 1$ defines an ellipsoid aligned with the coordinate axes with semiprincipal axes lengths $1/\sqrt{\lambda_1}$, $1/\sqrt{\lambda_2}$, and $1/\sqrt{\lambda_3}$, Khairuddin and Lionheart [23] proposed a strategy for determining an equivalent ellipsoid, which has the same Pólya–Szegö polarization tensor as the object under consideration.

Less is known for the case of the conducting (permeable) ellipsoid in the eddy-current regime. An analytical solution for conducting (permeable) prolate (and oblate) spheroids is available [7], but, for numerical calculation, they require truncation of an, otherwise, infinitely sized linear system. An approximate solution approach for the conducting permeable spheroids [8] and ellipsoids [17] has been proposed, but is limited to the case where the objects have small skin depths. To the best of our knowledge, an analytical solution for the general ellipsoid is not available. Thus, an extension of the approach of [23] to conducting ellipsoids is not immediate.

In Fig. 4, we show an illustration of the dependence of the diagonal coefficients of $\widetilde{\widetilde{\mathcal{M}}}$ with frequency for a prolate spheroid defined as $a = 0.02$ m, $b = c = 0.01$ m, $\sigma_* = 1.5 \times 10^7$ S/m, and $\mu_* = \mu_0$. We include the comparisons between the analytical solution of [7],[6] the converged numerical solution obtained by performing a frequency sweep using the approach [28], based on an unstructured grid of 14 579 tetrahedra and uniform $p = 3$ elements, and $\mathcal{T}(0)$ as the limit of the quasi-static approximation. For the purpose of numerical calculation, we truncate the computational domain at $100|B|$ and employ the NETGEN mesh generator for this and other meshes used generated in this paper [40]. Following Remark 13, we compute the shape-dependent constants according to [39], and establish that the quasi-static model remains valid for this spheroid provided that $f = \omega/(2\pi) \ll 5.4$ MHz.

The real part of the diagonal coefficients of $\widetilde{\widetilde{\mathcal{M}}}$ resembles a sigmoid function, whereas the imaginary part of the coefficients has a peak value $\sim$2 kHz and vanishes for low and high frequencies. The coefficients for the real part of $\widetilde{\widetilde{\mathcal{M}}}$ tend to zero at low frequencies and tend to those of $\mathcal{T}(0)$ at high frequencies. Thus, agreeing with the theoretical predictions in Section V. The agreement between the numerical prediction and the analytical solution is excellent.

Fig. 5 shows the corresponding dependence of the diagonal coefficients of $\widetilde{\widetilde{\mathcal{M}}}$ with frequency for the same-sized spheroid considered in Fig. 4, but now with $\sigma_* = 1.5 \times 10^7$ S/m and $\mu_* = 1.5\ \mu_0$. Applying the results of [39], we establish that the quasi-static model remains valid for this case provided that $f = \omega/(2\pi) \ll 3.6$ MHz.

The imaginary parts of $\widetilde{\widetilde{\mathcal{M}}}$ vanish for low-and high-frequency limits and the coefficients of the real part tend to the coefficients of $\mathcal{T}(\mu_r)$ and $\mathcal{T}(0)$, respectively, as expected. As with the case shown in Fig. 4, the agreement between the numerically computed tensor coefficients using a mesh of 14 579 unstructured tetrahedra and uniform $p = 3$ elements and the analytical solution is excellent.

VII. Results for Multiply Connected Objects

We first consider a solid torus with major and minor radii, 0.02 and 0.01 m, respectively, and material properties $\sigma_* = 5.96 \times 10^7$ S/m and $\mu_* = 1.5\ \mu_0$. In order to investigate the frequency response, we perform a frequency sweep, using the approach of [28], and consider the converged

[6]The analytical solution for the magnetic polarizability tensor, in this case, is not a closed-form expression, but instead requires computational truncation of an, otherwise, infinite system.

This article has been accepted for publication in a future issue of this journal, but has not been fully edited. Content may change prior to final publication. Citation information: DOI 10.1109/TMAG.2015.2507169, IEEE Transactions on Magnetics

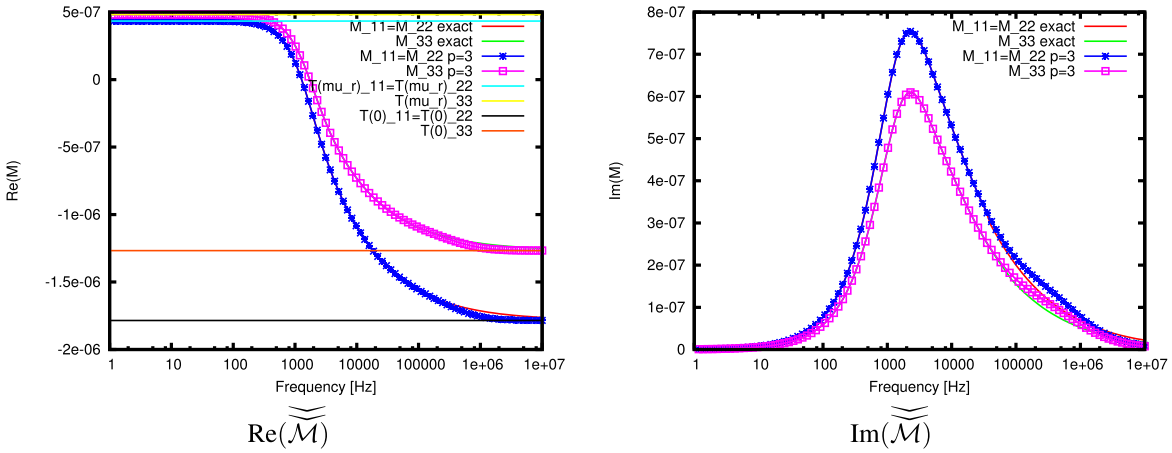

Fig. 5. Frequency response of a conducting permeable spheroid with $a = 0.02$ m, $b = c = 0.01$ m with $\sigma_* = 1.5 \times 10^7$ S/m, $\mu_* = 1.5\ \mu_0$ showing the diagonal coefficients of $\overleftrightarrow{\mathcal{M}}$ based on the analytical solution in [7], the numerically computed coefficients using the approach of [28] with an unstructured grid of 14 579 tetrahedra and uniform $p = 3$ elements, and the limiting $\mathcal{T}(\mu_r)$ and $\mathcal{T}(0)$ coefficients.

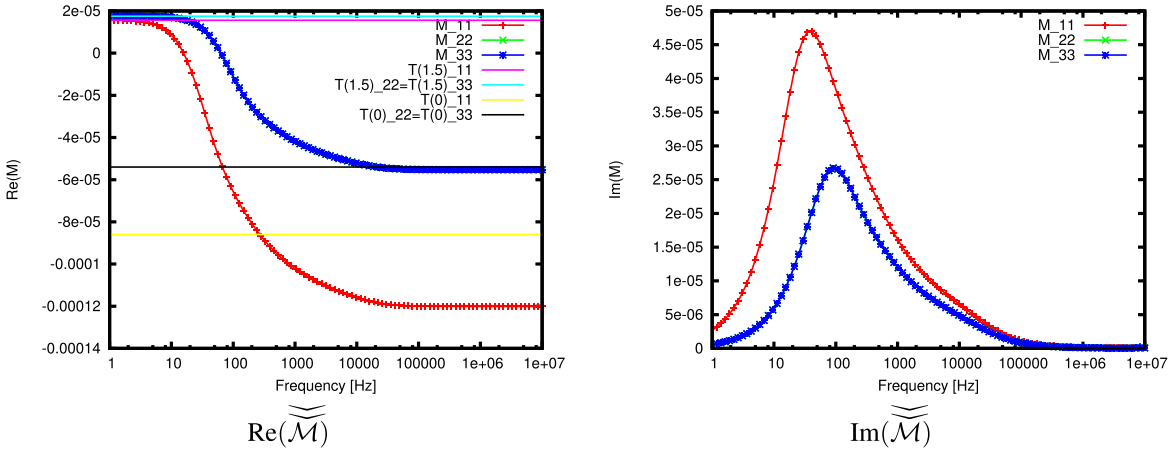

Fig. 6. Frequency response of a conducting permeable torus with major and minor radii, 0.02 and 0.01 m, respectively, and material properties $\sigma_* = 5.96 \times 10^7$ S/m and $\mu_* = 1.5\ \mu_0$ showing the coefficients of $\overleftrightarrow{\mathcal{M}}$ obtained using the approach of [28] with an unstructured grid of 29 882 tetrahedra and uniform $p = 2$ elements, and the limiting $\mathcal{T}(\mu_r)$, and $\mathcal{T}(0)$ coefficients.

non-zero coefficients of $\overleftrightarrow{\mathcal{M}}$ obtained with $p = 2$ on a mesh of 29 882 unstructured tetrahedra, which is generated in order to discretize the (unit sized) object and the region between the object and a spherical outer boundary with radius $100|B|$. The results of the frequency sweep are shown in Fig. 6, where we include, as a comparison, the non-zero coefficients of $\mathcal{T}(\mu_r)$ and $\mathcal{T}(0)$, which have also been computed numerically. Note that by computing the shape-dependent constants according to [39], we establish that the quasi-static model remains valid for this object provided that $f = \omega/(2\pi) \ll 12.2$ MHz.

Despite the fact that this object is multiply connected, with $\beta_0(B) = \beta_1(B) = 1$ and $\beta_2(B) = 0$, the low-frequency coefficients of $\overleftrightarrow{\mathcal{M}}$ still tend to those of $\mathcal{T}(\mu_r)$, as expected by Theorem 9. However, we do not expect the coefficients of $\overleftrightarrow{\mathcal{M}}$ to tend to $\mathcal{T}(0)$ as the high limit of quasi-static model is approach, as discussed in Remark 13, and our numerical experiments confirm that this is indeed a sufficient condition, since $\overleftrightarrow{\mathcal{M}}_{11} \nrightarrow \mathcal{T}(0)_{11}$, although, interestingly, $\overleftrightarrow{\mathcal{M}}_{22} = \overleftrightarrow{\mathcal{M}}_{33} \rightarrow \mathcal{T}(0)_{22} = \mathcal{T}(0)_{33}$ indicating a deeper result not covered by the earlier theory.

Second, we consider a sphere of radius 0.01 m with a spherical void of 0.005 m located centrally and the same material parameters as the above torus. We employ an unstructured mesh of 6873 tetrahedra with higher order geometry representation and present the converged results obtained for the frequency sweep of the non-zero diagonal coefficients of $\overleftrightarrow{\mathcal{M}}$ obtained with $p = 2$ elements. As in the case of the torus, a spherical outer boundary with radius $100|B|$ is used to truncate the computational domain. The results of the frequency sweep are shown in Fig. 7, where we include, as a comparison, the non-zero coefficients of $\mathcal{T}(\mu_r)$ and $\mathcal{T}(0)$, which have also been computed numerically. For this object, $\beta_0(B) = \beta_2(B) = 1$ and $\beta_1(B) = 0$, so that Theorem 9 holds in the low-frequency case and by Remark 13, $\overleftrightarrow{\mathcal{M}}$ tends to $\mathcal{T}(0)$ at the high frequency, as shown in Fig. 7. Note that the quasi-static model remains valid for this object provided that $f = \omega/(2\pi) \ll 12.8$ MHz.

This article has been accepted for publication in a future issue of this journal, but has not been fully edited. Content may change prior to final publication. Citation information: DOI 10.1109/TMAG.2015.2507169, IEEE Transactions on Magnetics

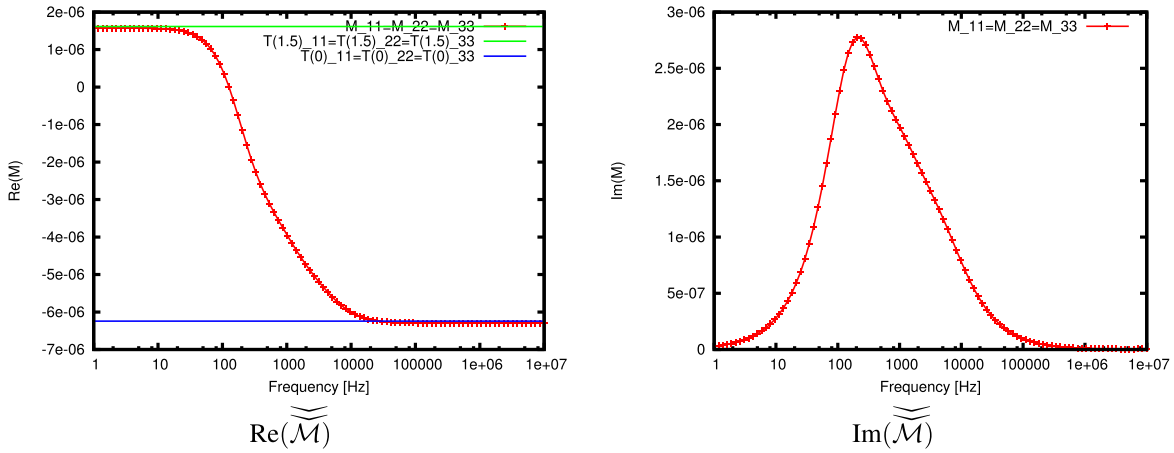

Fig. 7. Frequency response of a conducting permeable sphere of raduis 0.01 m with a centrally placed void of raduis 0.005 m, respectively, and material properties $\sigma_* = 5.96 \times 10^7$ S/m and $\mu_* = 1.5\ \mu_0$ showing the coefficents of $\overleftrightarrow{\mathcal{M}}$ obtained using the approach of [28] with an unstructured grid of 6873 tetrahedra and uniform $p = 2$ elements, and the limiting $\mathcal{T}(\mu_r)$ and $\mathcal{T}(0)$ coefficients.

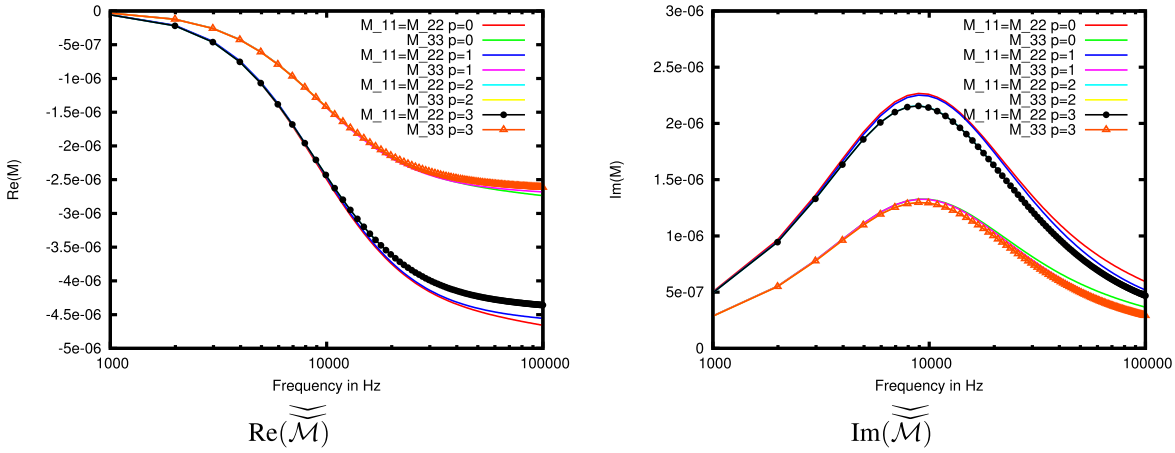

Fig. 8. Frequency response of a conducting Remington rifle cartridge as defined in [38] showing the diagonal coefficients of $\overleftrightarrow{\mathcal{M}}$ computed numerically using the approach of [28] with an unstructured grid of 23 551 tetrahedra and uniform $p = 0, 1, 2, 3$ elements.

VIII. Results for the Remington Rifle Cartridge

Adopting the simplified geometry and the material parameters according to the description of the Remington rifle cartridge given in [38], a mesh of 23 551 unstructured tetrahedra is generated in order to discretize the (unit sized) conducting object B and the region between the object and a rectangular outer bounding box $(-1000, 1000)^3$. The Remington rifle cartridge is positioned so that its length is aligned with the $\hat{\boldsymbol{e}}_3$ axis and the cylindrical cross section lies in the $\hat{\boldsymbol{e}}_1$ and $\hat{\boldsymbol{e}}_2$ plane, thus, due to the objects rotational and reflectional symmetries, $\overleftrightarrow{\mathcal{M}}$ is diagonal [28] with independent coefficients $\overleftrightarrow{\mathcal{M}}_{11} = \overleftrightarrow{\mathcal{M}}_{22}$ and $\overleftrightarrow{\mathcal{M}}_{33}$. The convergence of the independent coefficients of the tensor obtained by employing uniform $p = 0, 1, 2$ and $p = 3$ elements in turn for a frequency sweep is shown in Fig. 8. We observe that increasing p yields convergence of the real and imaginary coefficients of $\overleftrightarrow{\mathcal{M}}$ with the frequency response for $p = 2$ and $p = 3$ being practically indistinguishable from each other. The curves bear considerable similar to the frequency response from a non-permeable conducting spheroid shown previously in Fig. 4. Note that by computing the shape-dependent constants according to [39], we establish that the quasi-static model remains valid for this object provided that $f = \omega/(2\pi) \ll 3$ MHz.

If the Remington rifle cartridge is rotated about an axis, then the coefficients of $\overleftrightarrow{\mathcal{M}}$ transform according to [28]

$$\overleftrightarrow{\mathcal{M}}'_{ij} = \mathcal{R}_{ik}\mathcal{R}_{j\ell}\overleftrightarrow{\mathcal{M}}_{k\ell} \tag{61}$$

where $\mathcal{R}$ is the rotation matrix of the transformation. In particular, for a rotation θ about the $\hat{\boldsymbol{e}}_2$ axis, the components of the transformed tensor are given in (62), shown at the bottom of the next page.

The frequency response for $4\pi\overleftrightarrow{\mathcal{M}}'_{33}$ with rotation through 360° and for frequencies ranging from 1 to 100 kHz is shown in Fig. 9. The corresponding rotation response for the same set of frequencies is shown in Fig. 10. We remark that the magnitude of the real part of the coefficients of $\overleftrightarrow{\mathcal{M}}$ increases with increasing frequency, while the imaginary part of the coefficients peaks at ∼10 kHz and decays away from smaller and larger frequencies.

This article has been accepted for publication in a future issue of this journal, but has not been fully edited. Content may change prior to final publication. Citation information: DOI 10.1109/TMAG.2015.2507169, IEEE Transactions on Magnetics

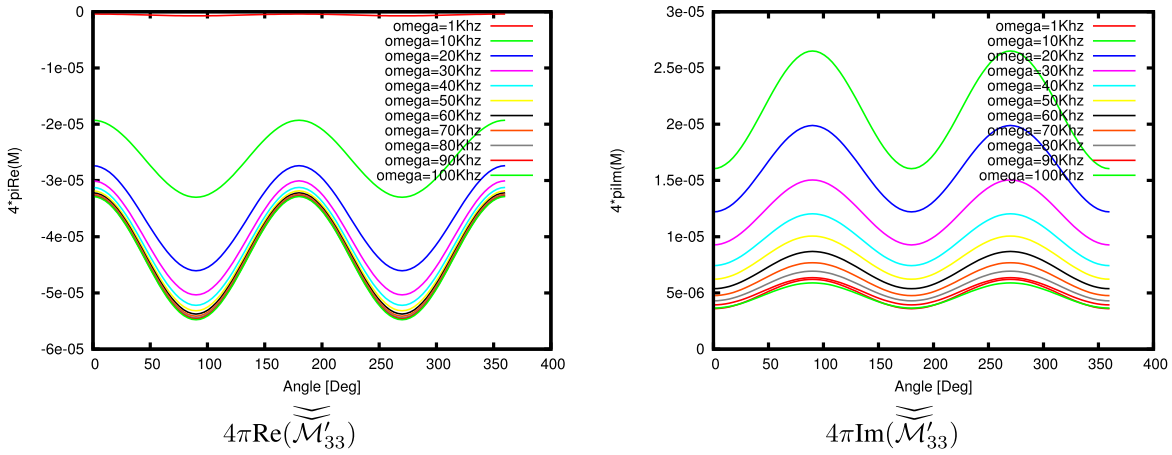

$4\pi\mathrm{Re}(\overleftrightarrow{\mathcal{M}}'_{33})$ $4\pi\mathrm{Im}(\overleftrightarrow{\mathcal{M}}'_{33})$

Fig. 9. Frequency response of a conducting Remington rifle cartridge as defined in [38] under rotation showing the transformed $4\pi\overleftrightarrow{\mathcal{M}}'_{33}$ for frequencies ranging from 1 to 100 kHz computed numerically using the approach of [28] with an unstructured grid of 23 551 tetrahedra and uniform $p = 3$ elements.

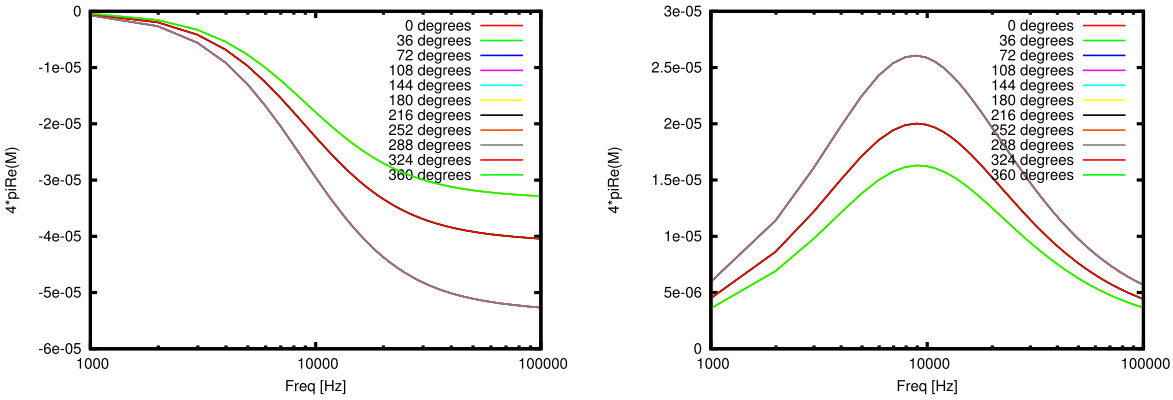

$4\pi\mathrm{Re}(\overleftrightarrow{\mathcal{M}}'_{33})$ $4\pi\mathrm{Im}(\overleftrightarrow{\mathcal{M}}'_{33})$

Fig. 10. Rotational response of a conducting Remington rifle cartridge as defined in [38] for different frequencies showing the transformed $4\pi\overleftrightarrow{\mathcal{M}}'_{33}$ for rotations ranging from 0° to 360° computed numerically using the approach of [28] with an unstructured grid of 23 551 tetrahedra and uniform $p = 3$ elements.

The results presented in Figs. 9 and 10 closely match the response of the measurements of the coefficients of $\overleftrightarrow{\mathcal{M}}$ to the changes in rotation and the changes in frequency presented in [31] for the same object.

IX. Conclusion

The properties of the rank 2 tensor $\overleftrightarrow{\mathcal{M}}$ and its connection with the Póyla–Szegö and the magnetic polarizability tensors have been investigated. We have described how our results in [28] provide a framework for the explicit computation of its coefficients. We have shown, by introducing a splitting of $\overleftrightarrow{\mathcal{M}}$, that a family of rank 2 tensors can be established, which describe the response from a range of magnetic and conducting objects. Furthermore, the bounds on the invariants of the Pólya–Szegö tensor have been established, and the low-frequency and high-conductivity limiting cases for the coefficients of $\overleftrightarrow{\mathcal{M}}$ have been obtained. We have also obtained the behavior of the coefficients for low conductivity and high frequencies at the limit of applicability of the quasi-static model, which are in agreement with the predictions in [27]. Interestingly, the connectedness of the object does not play a role in either the low-frequency or the low-conductivity case, but does in the high-frequency and high-conductivity cases. The results have been applied to ellipsoidal objects, multiply connected objects as well as the frequency and rotational responses from a Remington rifle cartridge.

Appendix
Engineering Connection

In this Appendix, we provide a connection between the engineering prediction of (1) and an asymptotic formula of

$$\overleftrightarrow{\mathcal{M}}' = \begin{pmatrix} \overleftrightarrow{\mathcal{M}}_{11}\cos^2\theta + \overleftrightarrow{\mathcal{M}}_{33}\sin^2\theta & 0 & \overleftrightarrow{\mathcal{M}}_{11}\cos\theta\sin\theta - \overleftrightarrow{\mathcal{M}}_{33}\cos\theta\sin\theta \\ 0 & \overleftrightarrow{\mathcal{M}}_{11} & 0 \\ \overleftrightarrow{\mathcal{M}}_{11}\cos\theta\sin\theta - \overleftrightarrow{\mathcal{M}}_{33}\cos\theta\sin\theta & 0 & \overleftrightarrow{\mathcal{M}}_{11}\cos^2\theta + \overleftrightarrow{\mathcal{M}}_{33}\sin^2\theta \end{pmatrix} \tag{62}$$

the form (20). Recall the Lorentz reciprocity principal, which is usually formulated for the time-harmonic equations, in the form [19], [27]

$$\nabla \cdot (\boldsymbol{E}^m \times \boldsymbol{H}^e - \boldsymbol{E}^e \times \boldsymbol{H}^m) = \boldsymbol{J}_0^m \cdot \boldsymbol{E}^e - \boldsymbol{J}_0^e \cdot \boldsymbol{E}^m \quad (63)$$

or by integrating over $\mathbb{R}^3$ and using the far field behavior of the fields, as

$$\int_{\mathbb{R}^3} \boldsymbol{J}_0^m \cdot \boldsymbol{E}^e d\boldsymbol{x} = \int_{\mathbb{R}^3} \boldsymbol{J}_0^e \cdot \boldsymbol{E}^m d\boldsymbol{x}. \quad (64)$$

It follows from this result that the response is unchanged when the transmitter and the receiver are interchanged. Furthermore, if the derivation is repeated for the eddy-current model, the result (64) is again obtained. Then, if we follow [27, pp. 300] and assume the current sources m and e to have a small support and to be located at $\boldsymbol{x}$ and $\boldsymbol{y}$, respectively, then the first term in a Taylor series of expansion of the fields $\boldsymbol{E}^m$ and $\boldsymbol{E}^e$ about the center of the current source[7] is

$$\boldsymbol{E}^e(\boldsymbol{x}) \cdot \boldsymbol{p}^m \approx \boldsymbol{E}^m(\boldsymbol{y}) \cdot \boldsymbol{p}^e \quad (65)$$

where $\boldsymbol{p}^m$ is the electric dipole moment of the current source m. It is important to note that this is only the first term in the Taylor's series expansion, including the next term leads to

$$\begin{aligned} &\boldsymbol{E}^e(\boldsymbol{x}) \cdot \boldsymbol{p}^m + 2\nabla^s \boldsymbol{E}^e(\boldsymbol{x}) : \mathcal{R}^m + \boldsymbol{B}^e(\boldsymbol{x}) \cdot \boldsymbol{m}^m \\ &\quad \approx \boldsymbol{E}^m(\boldsymbol{y}) \cdot \boldsymbol{p}^e + 2\nabla^s \boldsymbol{E}^m(\boldsymbol{y}) : \mathcal{R}^e + \boldsymbol{B}^m(\boldsymbol{y}) \cdot \boldsymbol{m}^e \end{aligned} \quad (66)$$

where $\mathcal{R}^m$ is a quadrupole moment of the current source m, $\boldsymbol{m}^m$ is the magnetic moment of the same current source [27] and exact reciprocity is expected if all the terms in the Taylor series expansion are considered.

For the eddy-current problem described in this paper and coils located in free space that can be idealized as dipoles with a magnetic moment, only, reciprocity implies that $\boldsymbol{m}^m \cdot \boldsymbol{H}_\alpha^e(\boldsymbol{x}) \approx \boldsymbol{m}^e \cdot \boldsymbol{H}_\alpha^m(\boldsymbol{y})$, i.e., the result is the same if $\boldsymbol{x}$ and $\boldsymbol{w}$ and $\boldsymbol{m}^m$ and $\boldsymbol{m}^e$ are interchanged. Considering (3), we have in vector notation

$$\begin{aligned} &\boldsymbol{m}^m \cdot \boldsymbol{H}_\alpha^e(\boldsymbol{x}) - \boldsymbol{m}^e \cdot \boldsymbol{H}_\alpha^m(\boldsymbol{y}) \\ &\quad = \boldsymbol{m}^m \cdot (\boldsymbol{D}^2 G(\boldsymbol{x}, z) \mathcal{A}(\boldsymbol{D}^2 G(z, \boldsymbol{y}) \boldsymbol{m}^e)) \\ &\qquad - \boldsymbol{m}^e \cdot (\boldsymbol{D}^2 G(\boldsymbol{y}, z) \mathcal{A}(\boldsymbol{D}^2 G(z, \boldsymbol{x}) \boldsymbol{m}^m)) \\ &\qquad + \Delta(\boldsymbol{m}^m, \boldsymbol{R}^e) - \Delta(\boldsymbol{m}^e, \boldsymbol{R}^m) \end{aligned} \quad (67)$$

where $\Delta(\boldsymbol{m}, \boldsymbol{R}) := \boldsymbol{m} \cdot \boldsymbol{R}$, and in the case considered, $\boldsymbol{H}_0^e(\boldsymbol{x}) = \boldsymbol{D}^2 G(\boldsymbol{x}, \boldsymbol{y}) \boldsymbol{m}^e$ and $\boldsymbol{H}_0^m(\boldsymbol{w}) = \boldsymbol{D}^2 G(\boldsymbol{y}, \boldsymbol{x}) \boldsymbol{m}^m$, thus, from the symmetry of $\boldsymbol{D}^2 G(\boldsymbol{x}, \boldsymbol{y})$, we have used $\boldsymbol{m}^m \cdot \boldsymbol{H}_0^e(\boldsymbol{x}) = \boldsymbol{m}^e \cdot \boldsymbol{H}_0^m(\boldsymbol{y})$. It follows from (12), [2], and [28] that:

$$\begin{aligned} &|\Delta(\boldsymbol{m}^m, \boldsymbol{R}^e) - \Delta(\boldsymbol{m}^e, \boldsymbol{R}^m)| \\ &\quad \leqslant |\boldsymbol{m}^m||\boldsymbol{R}^e(\boldsymbol{x})| + |\boldsymbol{m}^e||\boldsymbol{R}^m(\boldsymbol{y})| \\ &\quad \leqslant C\alpha^4 \big(|\boldsymbol{m}^m| \|\boldsymbol{H}_0^e\|_{W^{2,\infty}(B_\alpha)} + |\boldsymbol{m}^e| \|\boldsymbol{H}_0^m\|_{W^{2,\infty}(B_\alpha)}\big). \end{aligned}$$

Thus, (67) is an asymptotic expansion for $\boldsymbol{m}^m \cdot \boldsymbol{H}_\alpha^e(\boldsymbol{x}) - \boldsymbol{m}^e \cdot \boldsymbol{H}_\alpha^m(\boldsymbol{y})$ as $\alpha \to 0$ with $\Delta(\boldsymbol{m}^m, \boldsymbol{R}^e) - \Delta(\boldsymbol{m}^e, \boldsymbol{R}^m) = O(\alpha^4)$. Then, upto this residual term

$$\begin{aligned} &\boldsymbol{m}^m \cdot (\boldsymbol{D}^2 G(\boldsymbol{x}, z) \mathcal{A}(\boldsymbol{D}^2 G(z, \boldsymbol{y}) \boldsymbol{m}^e)) \\ &\qquad \approx \boldsymbol{m}^e \cdot (\boldsymbol{D}^2 G(\boldsymbol{y}, z) \mathcal{A}(\boldsymbol{D}^2 G(z, \boldsymbol{x}) \boldsymbol{m}^m)). \end{aligned} \quad (68)$$

[7] As the size of support of the sources relative to the wavelength, the distance between them tends to zero.

In light of (64), if one constructs a suitable $\boldsymbol{J}_0^m$, which has non-zero support on the measurement coil and is such that the resulting field $\boldsymbol{H}_0^m$ can be idealized as a magnetic dipole, the induced voltage, V^{ind}, as a result of the perturbation caused by the presence of a general conducting object, is

$$\begin{aligned} V^{\text{ind}} &\approx C\boldsymbol{m}^m \cdot (\boldsymbol{D}^2 G(\boldsymbol{x}, z) \mathcal{A}(\boldsymbol{D}^2 G(z, \boldsymbol{y}) \boldsymbol{m}^e)) \\ &\approx C\boldsymbol{H}_0^m(z) \cdot (\mathcal{A}\boldsymbol{H}_0^e(z)) \end{aligned} \quad (69)$$

up to a scaling constant C.

ACKNOWLEDGMENT

This work was supported in part by the Engineering and Physical Sciences Research Council under Grant EP/K00428X/1 and Grant EP/K039865/1 and in part by the Land Mine Research Charity Find A Better Way. The authors would like to thank Prof. H. Ammari, J. Chen, A. J. Peyton, and D. Volkov for their helpful discussions and comments on polarizability tensors, and to thank Dr. K. Schmidt for the help with the calculation of shape-dependent constants to deduce the limit of the quasi-static model.

REFERENCES

[1] H. Ammari, A. Buffa, and J. C. Nédélec, "A justification of eddy currents model for the Maxwell equations," *SIAM J. Appl. Math.*, vol. 60, no. 5, pp. 1805–1823, 2000.

[2] H. Ammari, J. Chen, Z. Chen, J. Garnier, and D. Volkov, "Target detection and characterization from electromagnetic induction data," *J. Math. Pures Appl.*, vol. 101, no. 1, pp. 54–75, Jan. 2014.

[3] H. Ammari, J. Chen, Z. Chen, D. Volkov, and H. Wang, "Detection and classification from electromagnetic induction data," *J. Comput. Phys.*, vol. 301, pp. 201–217, Nov. 2015.

[4] H. Ammari and H. Kang, *Polarization and Moment Tensors: With Applications to Inverse Problems and Effective Medium Theory*. New York, NY, USA: Springer, 2007.

[5] H. Ammari, M. S. Vogelius, and D. Volkov, "Asymptotic formulas for perturbations in the electromagnetic fields due to the presence of inhomogeneities of small diameter II. The full Maxwell equations," *J. Math. Pures Appl.*, vol. 80, no. 8, pp. 769–814, Oct. 2001.

[6] H. Ammari and D. Volkov, "The leading-order term in the asymptotic expansion of the scattering amplitude of a collection of finite number of dielectric inhomogeneities of small diameter," *Int. J. Multiscale Comput. Eng.*, vol. 3, no. 3, pp. 285–296, 2005.

[7] C. O. Ao, H. Braunisch, K. O'Neill, and J. A. Kong, "Quasi-magnetostatic solution for a conducting and permeable spheroid with arbitrary excitation," *IEEE Trans. Geosci. Remote Sens.*, vol. 40, no. 4, pp. 887–897, Apr. 2002.

[8] B. E. Barrowes, K. O'Neill, T. M. Grzegorczyk, X. Chen, and J. A. Kong, "Broadband analytical magnetoquasistatic electromagnetic induction solution for a conducting and permeable spheroid," *IEEE Trans. Geosci. Remote Sens.*, vol. 42, no. 11, pp. 2479–2489, Nov. 2004.

[9] C. E. Baum, "Low-frequency near-field magnetic scattering from highly, but not perfectly, conducting bodies," Phillips Lab., Kirtland, OH, USA, Tech. Rep. 499, 1993.

[10] C. E. Baum, "The magnetic polarizability dyadic and point symmetry," Phillips Lab., Kirtland, OH, USA, Tech. Rep. 502, 1994.

[11] A. Bossavit, "Magnetostatic problems in multiply connected regions: Some properties of the curl operator," *IEE Proc. A, Phys. Sci., Meas. Instrum., Manage. Edu.-Rev.*, vol. 135, no. 3, pp. 179–187, Mar. 1988.

[12] Y. Capdeboscq and M. S. Vogelius, "Optimal asymptotic estimates for the volume of internal homogeneities in terms of multiple boundary measurements," *Math. Model. Numer. Anal.*, vol. 37, no. 2, pp. 227–240, 2003.

[13] D. J. Cedio-Fengya, S. Moskow, and M. S. Vogelius, "Identification of conductivity imperfections of small diameter by boundary measurements. Continuous dependence and computational reconstruction," *Inverse Problems*, vol. 14, pp. 553–595, 1998.

[14] Y. Das, J. E. McFee, J. Toews, and G. C. Stuart, "Analysis of an electromagnetic induction detector for real-time location of buried objects," *IEEE Trans. Geosci. Remote Sens.*, vol. 28, no. 3, pp. 278–288, May 1990.
[15] G. Dassios and R. E. Kleinman, *Low Frequency Scattering*. Oxford, U.K.: Oxford Science, 2000.
[16] P. Gaydecki, I. Silva, B. T. Fernandes, and Z. Z. Yu, "A portable inductive scanning system for imaging steel-reinforcing bars embedded within concrete," *Sens. Actuators A, Phys.*, vol. 84, nos. 1–2, pp. 25–32, Aug. 2000.
[17] T. M. Grzegorczyk, B. Zhang, J. A. Kong, B. E. Barrowes, and K. O'Neill, "Electromagnetic induction from highly permeable and conductive ellipsoids under arbitrary excitation: Application to the detection of unexploded ordnances," *IEEE Trans. Geosci. Remote Sens.*, vol. 46, no. 4, pp. 1164–1176, Apr. 2008.
[18] H. Griffiths, "Magnetic induction tomography," in *Electrical Impedance Tomography: Methods, History and Applications*, D. S. Holder, Ed. Bristol, U.K.: IOP Publishing, 2005, pp. 213–238.
[19] R. F. Harrington, *Time-Harmonic Electromagnetic Fields*. London, U.K.: McGraw-Hill, 1961.
[20] J. D. Jackson, *Classical Electrodynamics*. New York, NY, USA: Wiley, 1967.
[21] A. Järvi, "Metallinilmaisimen Mallintaminen Ja Kehittäminen (in Finish)," M.S. thesis, Helsinki Univ. Technol., Espoo, Finland, 1989.
[22] J. B. Keller, R. E. Kleinman, and T. B. A. Senior, "Dipole moments in Rayleigh scattering," *J. Inst. Math. Appl.*, vol. 9, no. 1, pp. 14–22, 1972.
[23] T. A. Khairuddin and W. R. B. Lionheart, "Fitting ellipsoids to objects by the first order polarization tensor," *Malaya J. Matematik*, vol. 1, pp. 44–53, Apr. 2013.
[24] R. E. Kleinman, "Far field scattering at low frequencies," *Appl. Sci. Res.*, vol. 18, no. 1, pp. 1–8, Jan. 1967.
[25] R. E. Kleinman, "Dipole moments and near field potentials," *Appl. Sci. Res.*, vol. 27, no. 1, pp. 335–340, Jan. 1973.
[26] R. E. Kleinman and T. B. A. Senior, "Rayleigh scattering," Univ. Michigian Radiat. Lab., Ann Arbor, MI, USA, Tech. Rep. RL 728, 1982.
[27] L. D. Landau and E. M. Lifshitz, *Electrodynamics of Continuous Media*, 1st ed. New York, NY, USA: Pergamon, 1960.
[28] P. D. Ledger and W. R. B. Lionheart, "Characterizing the shape and material properties of hidden targets from magnetic induction data," *IMA J. Appl. Math.*, vol. 80, no. 6, pp. 1776–1798, 2015.
[29] P. D. Ledger and W. R. B. Lionheart, "The perturbation of electromagnetic fields at distances that are large compared with the object's size," *IMA J. Appl. Math.*, vol. 80, no. 3, pp. 865–892, 2015.
[30] P. D. Ledger and S. Zaglmayr, "*hp* finite element simulation of three-dimensional eddy current problems on multiply connected domains," *Comput. Methods Appl. Mech. Eng.*, vol. 199, nos. 49–52, pp. 3386–3401, Dec. 2010.
[31] L. A. Marsh, C. Ktistis, A. Järvi, D. W. Armitage, and A. J. Peyton, "Three-dimensional object location and inversion of the magnetic polarizability tensor at a single frequency using a walk-through metal detector," *Meas. Sci. Technol.*, vol. 24, no. 4, p. 045102, 2013.
[32] G. W. Milton, *The Theory of Composites*. Cambridge, U.K.: Cambridge Univ. Press, 2002.
[33] P. Monk, *Finite Element Methods for Maxwell's Equations*. London, U.K.: Oxford Univ. Press, 2003.
[34] P. M. Morse and H. Feshbach, *Methods of Theoretical Physics*, vol. 2. New York, NY, USA: McGraw-Hill, 1953.
[35] S. J. Norton and I. J. Won, "Identification of buried unexploded ordnance from broadband electromagnetic induction data," *IEEE Trans. Geosci. Remote Sens.*, vol. 39, no. 10, pp. 2253–2261, Oct. 2001.
[36] J. A. Osborn, "Demagnetizing factors of the general ellipsoid," *Phys. Rev.*, vol. 67, pp. 351–357, Jun. 1945.
[37] L. R. Pasion and D. W. Oldenburg, "Locating and characterizing unexploded ordnance using time domain electromagnetic induction," U.S. Army Environ. Res. Develop. Centre, Vicksburg, MS, USA, Tech. Rep. ERDC/GSL TR-01-10, 2001.
[38] O. A. Abdel Rehim, J. L. Davidson, L. A. Marsh, M. D. O'Toole, D. W. Armitage, and A. J. Peyton, "Measurement system for determining the magnetic polarizability tensor of small metal targets," in *Proc. IEEE Sensor Appl. Symp.*, Apr. 2015, pp. 1–5.
[39] K. Schmidt, O. Sterz, and R. Hiptmair, "Estimating the eddy-current modeling error," *IEEE Trans. Magn.*, vol. 44, no. 6, pp. 686–689, Jun. 2008.
[40] J. Schöberl, "NETGEN an advancing front 2D/3D-mesh generator based on abstract rules," *Comput. Visualizat. Sci.*, vol. 1, no. 1, pp. 41–52, Jul. 1997. [Online]. Available: http://sourceforge.net/projects/netgen-mesher/
[41] J. Simmonds and P. Gaydecki, "Defect detection in embedded reinforcing bars and cables using a multi-coil magnetic field sensor," *Meas. Sci. Technol.*, vol. 10, no. 7, pp. 640–648, 1999.
[42] M. Soleimani, W. R. B. Lionheart, and A. J. Peyton, "Image reconstruction for high-contrast conductivity imaging in mutual induction tomography for industrial applications," *IEEE Trans. Instrum. Meas.*, vol. 56, no. 5, pp. 2024–2032, Oct. 2007.
[43] R. C. Thompson, "Singular values and diagonal elements of complex symmetric matrices," *Linear Algebra Appl.*, vol. 26, pp. 65–106, Aug. 1979.
[44] R. J. Wait, "A conducting sphere in a time varying magnetic field," *Geophysics*, vol. 16, no. 4, pp. 666–672, 1951.
[45] F. Watson, "Better imaging for landmine detection: An exploration of 3d full-wave inversion for ground penetrating radar," Ph.D. dissertation, School Math., Univ. Manchester, Oxford, U.K., 2015.
[46] M. Zolgharni, P. D. Ledger, D. W. Armitage, D. Holder, and H. Griffiths, "Imaging cerebral haemorrhage with magnetic induction tomography: Numerical modelling," *Physiol. Meas.*, vol. 30, no. 6, pp. 187–200, 2009.

Paul D. Ledger received the B.Eng. degree in civil engineering with computational mechanics from the University of Birmingham, Birmingham, U.K., in 1998, and the M.Sc. degree in computational modeling and finite elements in engineering mechanics and the Ph.D. degree in hp-finite elements for electromagnetic scattering from Swansea University, Wales, U.K., in 1999 and 2002, respectively.

He is currently an Associate Professor with the College of Engineering, Swansea University. His current research interests include high order/hp-finite elements applied to problems in computational electromagnetism, error estimation, and adaptivity, and the computational solution of coupled and inverse problems.

William R. B. Lionheart received the B.Sc. degree in applied mathematics from The University of Warwick, Coventry, U.K., in 1980, and the Ph.D. degree in electrical impedance tomography from Oxford Brookes University, Oxford, U.K., in 1990.

He has worked on a wide range of inverse problems in medicine and industry including electrical impedance tomography, magnetic induction tomography, X-ray CT, and PET. His interest in low frequency electromagnetic imaging leads to his involvement in the civilian land mine clearance charity Find a Better Way, which he was involved in founding and sits on the Scientific and Users Advisory Panel. He is currently a Professor of Applied Mathematics with The University of Manchester; Manchester, U.K.

Prof. Lionheart was a recipient of the Royal Society's 2015 Wolfson Research Merit Award for Novel Methods in Tomography Imaging: Rich Tomography and Fast Dynamic Imaging.